

SI Appendix: Table of contents

<u>List of Supplementary tables, figures and datasets</u>	2
<u>Supplementary Information</u>	3
1. Enhancements of the reconstructed <i>Synechocystis</i> network	3
- Photosynthetic specific pathways	3
- Lipids modeling	4
- Transport reactions	5
- Mass and charge balance	7
- Biomass reactions	8
2. iJN678 represents a database of current biochemical, genetic and genomic knowledge about <i>Synechocystis</i>	10
3. Computation of the <i>Synechocystis</i> growth rate	11
4. Internal flux distributions: prediction and validation	13
5. Study of proton flux exchange in <i>Synechocystis</i>	20
6. Metabolic robustness and gene essentiality study of <i>iJN678</i>	22
7. Analysis of the heterotrophic metabolism of <i>Synechocystis</i>	25
<u>Supplementary Methods</u>	28
1. Metabolic reconstruction	28
2. Biomass reactions formulation	30
3. Conversion of the reconstruction into a mathematical model	30
4. Analysis of metabolic flux	31
5. Formulation of <i>iBG-11</i> minimal medium	32
6. Simulation constraints	32
- Growth rate performance	32
- Study of proton flux exchange in <i>Synechocystis</i>	33
- Expansion of the known array of carbon and nitrogen sources that support growth	33
7. Gene essentiality and synthetic lethality analysis	33
8. Simplified model and constraints used for photosynthesis analysis	34
9. Robustness analysis of photosynthesis	37
10. Estimation of ATP/NADPH ratio	39
11. Sequence data analysis	41
<u>Supplementary References</u>	42

List of Supplementary tables, figures and datasets

Supplementary tables

Table S1. Characteristics of the reconstructed metabolic network of <i>Synechocystis</i>	9
Table S2. Comparison of <i>iJN678</i> with previous metabolic reconstruction from <i>Synechocystis</i>	9
Table S3. Comparison of growth rates of the <i>in silico</i> strain <i>iJN678</i> and <i>Synechocystis</i>	12
Table S4. Comparison of <i>in silico</i> growth prediction with <i>in vivo</i> experimental data	26
Table S5. Potential new carbon sources for <i>Synechocystis</i>	27

Supplementary figures

Figure S1. Modeling of the oxidative phosphorylation and photosynthetic pathways included in <i>iJN678</i>	4
Figure S2. Transport modeling	6
Figure S3. A comprehensive knowledge base that summarizes and categorizes the information currently available for <i>Synechocystis</i>	11
Figure S4. <i>Synechocystis</i> growth under autotrophic conditions	13
Figure S5. Flux distribution predicted under heterotrophic conditions	15
Figure S6. Flux distribution predicted under autotrophic conditions	17
Figure S7. Flux distribution predicted under mixotrophic conditions	19
Figure S8. Effect of proton exchange on predicted growth rate	21
Figure S9. Gene essentiality and synthetic lethality analysis of <i>Synechocystis</i>	24
Figure S10. Futile metabolic cycle proposed for ATP/ADP balancing in <i>Synechocystis</i> under CLS	28
Figure S11. Robustness analysis of photosynthesis	38

Datasets

Dataset S1. Reactions, metabolites, references and main statistics from <i>iJN678</i>	
Dataset S2. Biomass objective function modeling	
Dataset S3. Flux distribution analysis by FBA	
Dataset S4. TCA cycle and GABA shunt analysis in cyanobacteria	
Dataset S5. Synthetic lethal and gene essentiality analysis	
Dataset S6. Photosynthesis optimality analysis	

Supplementary Information

1. Enhancements of the reconstructed *Synechocystis* network

The properties of *Synechocystis* PCC8063 genome-scale reconstruction are shown in Table S1. The major areas of enhancement over previous metabolic reconstructions of *Synechocystis* are summarized in Table S2 and are as follows:

Photosynthetic specific pathways. We modeled in detail oxidative phosphorylation and the photosynthetic apparatus of *Synechocystis* by taking into account that, while the thylakoid membrane contains both photosynthetic and respiratory electron transport chains, only the respiratory chain is present in the cytoplasmic membrane (Fig. S1) (1). The oxidative phosphorylation pathway includes NDH-1, NDH-2, NDH-1₃, and NDH-1₄ NAD(P)H dehydrogenase complexes (2), the membrane-associated succinate dehydrogenase complex SDH (1), two aa3-type terminal oxidases (CtaI and CtaII, CYO) (3), and the plastoquinone oxidase (CydBD) (3), together with ATPase complexes (4). The photosynthetic electron chain includes photosystem II (PSII), cytochrome b₆f (CYTBF), photosystem I (PSI), and the ferredoxin NADP⁺ oxidoreductase (FNR) as components of the linear electron chain (LEF) (4). In addition, the ferredoxin plastoquinone reductase (FQR) reaction was included (5, 6). Auxiliary photosynthetic electron transport pathways, such as the MEHLER reaction (7) and the bidirectional hydrogenase (8) were also included in the reconstructed photosynthetic apparatus (Fig. S1). Based on the presence of an efficient inorganic carbon concentration mechanism in *Synechocystis* (9), it was assumed that cyanobacteria do not possess photorespiration. However, recent reports have shown that an active photorespiratory metabolism is present in *Synechocystis*, employing a plant-like glycolate cycle, a bacterial-like glycerate pathway, and complete decarboxylation of glyoxylate *via* formate (10). The three photorespiratory pathways were included in the metabolic reconstruction. Another important set of pathways, included are those involved in the synthesis of photosynthetic pigments. *iJN678* contains complete biosynthetic pathways for chlorophyll a, lycopene, and other carotenoid compounds, including β -carotenoids, zeaxanthin, and equinone. Biosynthetic pathways for α -, β -, γ - and δ -tocopherol were also included. Beyond their role in photosynthesis (11, 12), these metabolites are of biotechnological interest as they have a high added value (13).

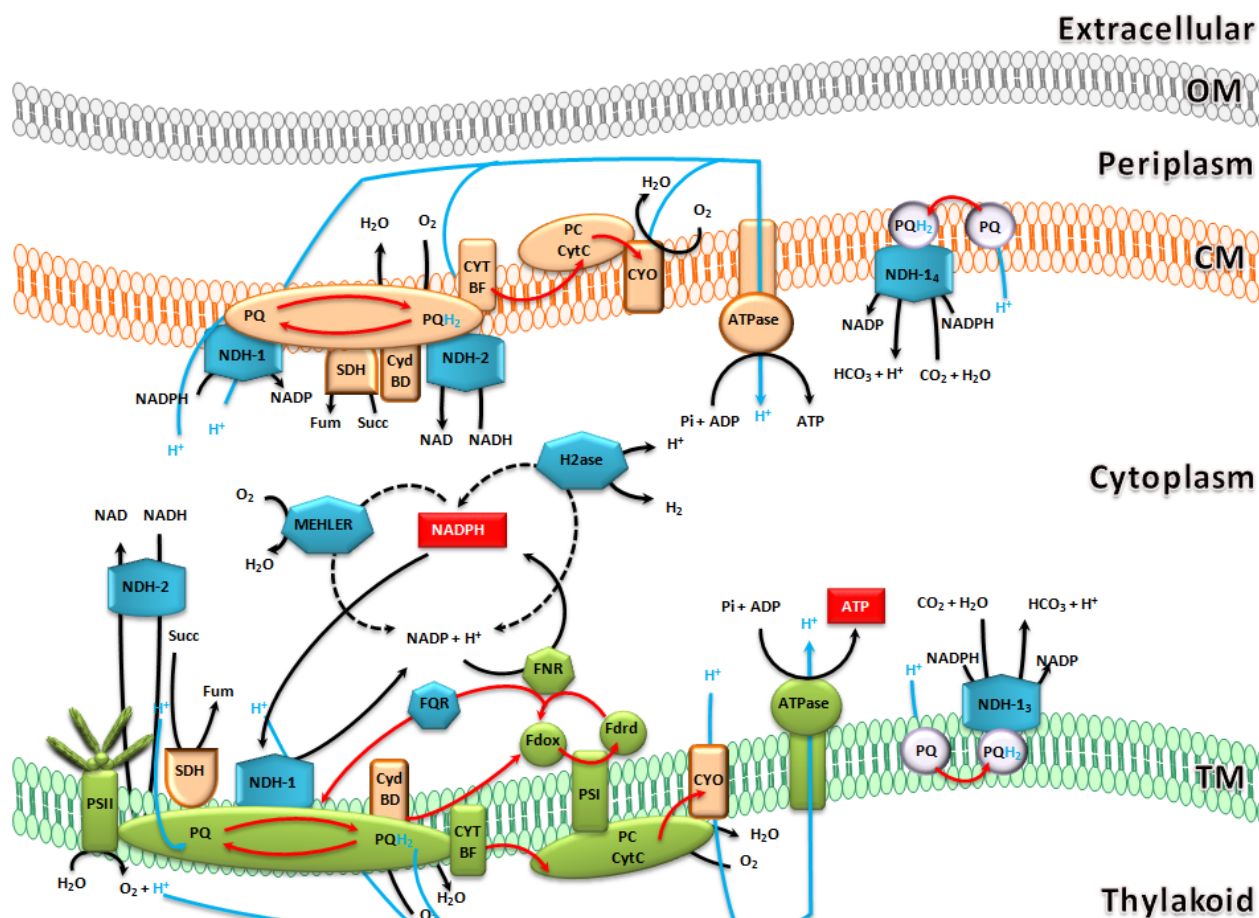


Figure S1. Modeling of the oxidative phosphorylation and photosynthetic pathways included in *iJN678*. The four compartments included in the reconstruction, i.e., extracellular, periplasm, cytoplasm and thylakoid separated by the outer (OM), cytoplasmatic (CM) and thylakoid (TM) membranes, are indicated. The photosynthetic linear electron flow (green) and the respiratory (orange) pathways as well as the accessory photosynthetic and respiratory branches (in blue) are placed in the right locations. The abbreviations used are: SDH, succinate dehydrogenase complex; PQ, plastoquinone; CYTBF, cytochrome $Cytb_6f$; PC, plastocyanine; CytC, cytochrome c_6 ; CYO, cytochrome oxidase; CYTBD, plastoquinone oxidase; PSI, photosystem I; Fdox, oxidized ferredoxin; Fdrd, reduced ferredoxin; FNR, ferredoxin $NADP^+$ reductase; FQR, ferredoxin plastoquinone reductase; H2ase, bidirectional hydrogenase; MEHLER, Mehler reaction; ATPase, ATP synthetase; NDH-1, NADPH dehydrogenase complex 1; NDH-2, NADH dehydrogenase; NDH-13, NADPH dehydrogenase complex 3; NDH-14, NADPH dehydrogenase complex 4. The flux of electrons and protons through the photosynthetic and respiratory pathways is indicated by red and blue arrows, respectively. The final photosynthetic products, i.e., ATP and NADPH, are shown by red squares.

Lipids modeling. Modeling of lipids biosynthetic pathways poses a real challenge in metabolic reconstructions due to the limited amount of information available. As a consequence, the fatty acid biosynthesis is often partially modeled and only the intermediates are included in the biomass objective function (14). Given the metabolic and biotechnological importance of fatty

acid biosynthesis in *Synechocystis* (15) and the fact that a wealth of information about lipids biosynthesis is available for *Synechocystis* (16), the four classes of lipids present in *Synechocystis* were modeled in detail. Thus, biosynthesis pathways were modeled for the glycolipids monogalactosyldiacylglycerol (MGDG), digalactosyldiacylglycerol (DGDG) and sulfolipids sulfolipids (SUL) and the phospholipid phosphatidylglycerol (PG) (Dataset S2). Acyl-lipid desaturase reactions were included on the basis of the genetic and biochemical information available (17). The model therefore accounts for many relevant polyunsaturated lipids, e.g., ω -3 fatty acids. A detailed list of fatty acids and lipids included in the reconstruction is shown in Dataset S2.

Transport reactions. Active transport appears to be the primary means by which microorganisms acquire organic carbon and other substrates from the environment. A detailed analysis of transport systems is therefore a first step in the study of the heterotrophic metabolism of a particular organism. Transport reactions have received limited attention in previous reconstructions of *Synechocystis* despite their critical roles in cell metabolism (18-22). These reactions largely determine the metabolites that can be used in the reconstruction as biomass precursors and energy sources. A total of five different inorganic carbon uptake systems have been identified in *Synechocystis*: three HCO_3^- transporters (the BicA, SbtA and BCT systems) and two CO_2 uptake systems mediated by the NDH-1₃ and NDH-1₄ dehydrogenase complexes (9). Several transporter systems for nitrogen (23), sulfur (24), phosphate (25), metals and other anions have been identified as well. Transport systems for neutral amino acids and histidine, for basic amino acids and glutamine as well as for glutamate, have also been identified (26). All of these transporters were included in the model, together with the well-known glucose and fructose transporter GlcP (27). Furthermore, non-gene-associated transport reactions for several organic acids such as pyruvate, oxoglutarate and citrate were included on the basis of experimental evidence (19, 28-30) (Dataset S1). It is important to note that no outer-membrane transporters are encoded in the genome of *Synechocystis* (<http://genome.kazusa.or.jp/cyanobase>). This suggests a high permeability of the *Synechocystis* outer membrane compared to other bacteria such as *Pseudomonas*, in which numerous outer membrane porins circumvent the low permeability of their outer membranes (31). Based on this assumption, the transport through the outer membrane was modeled by using passive diffusion transport reactions (Dataset S1).

A total of 221 genes encoding 168 potential transporters have been predicted in *Synechocystis* (<http://www.membranetransport.org/>), implying 47.06 transporters per Mb of genome, a significantly smaller number of transporters compared with other metabolic versatile gram-negative bacteria such as *E. coli* and *P. putida* KT2440, 76.96 and 63.28 transporters per Mb respectively (<http://www.membranetransport.org/>). A functional classification of the genes encoding for transporters in the *Synechocystis* genome showed, as expected for a photosynthetic microorganism, that more than 50% are involved in the uptake of inorganic metabolites (Fig. S2). Interestingly, 10% of the transporters in *Synechocystis* encode for putative sugar and organic acid transporters and approximately 12% are involved in amino acid uptake systems, suggesting an important role of heterotrophic metabolism in this cyanobacterium. A comparison of the genes encoding for transporters encoded in the *Synechocystis* genome and those that were included in *iJN678* is shown in Fig. S2.

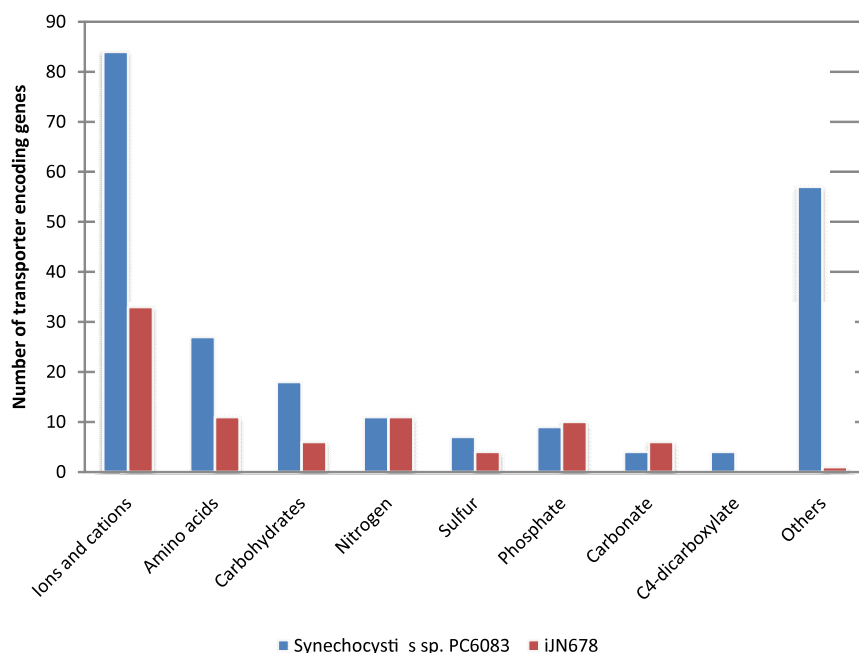


Figure S2. Transport modeling. Predicted transporter-encoding genes in *Synechocystis* (blue bars) compared with the transporter-encoding genes included in *iJN678* (red bars).

Mass and charge balance. Environmental changes, such as variations in pH, temperature or osmolarity, can alter the trans-membrane proton motive force and consequently affect the internal homeostasis of the cell as well as the energy production. In order to maintain internal homeostasis, cells have to regulate the internal pH by secreting or consuming protons in steady-state conditions. Reactions in *iJN678* are completely mass and charge balanced in contrast to previous metabolic reconstructions (19, 20, 22) of *Synechocystis* and account for all the protons being generated and consumed; thus, the internal and external proton balancing can be investigated *in silico* (32), see below.

Biomass reaction. The formulation of a detailed biomass objective function (BOF) in a metabolic reconstruction is critical for model evaluation and quantitative predictions and realistic gene essentiality analysis (33). The BOFs included in previous *Synechocystis* reconstructions account mainly for amino acid, fatty acid and nucleic acid precursors (18-22). The biomass presented here accounts for the major biomass constituents and their fractional contributions to the overall cellular biomass. It was derived from the literature and estimated from genomic content, Dataset S2.

A brief comparison between *iJN678* and the available *Synechocystis* reconstructions is provided in table S2. In addition, we performed a quantitative and qualitative comparison between *iJN678* and *iSyn699* (22) and *iSyn811* (21), recently published *Synechocystis* metabolic reconstructions. Since the gene content of *iSyn811* is not publicly available, we only carried out gene content comparison between *iJN678* and *iSyn699* (22). We found that a total of 567 genes are included in both reconstructions, 170 genes are only included in *iJN678* and 80 genes are only present in *iSyn669* (Dataset S1). Genes exclusive to *iJN678* encode mainly for reactions involved in photosynthesis, oxidative phosphorylation, photo-respiration, lipids and photosynthetic pigments biosynthesis, transport and *Synechocystis*-specific storage polymers, such as cyanophycin and poly-hydroxybutyrate (Dataset S1). On the other hand, reactions associated with genes only present in *iSyn669* include biosynthetic pathways not included in *iJN678* such as lipoic acid, DNA and RNA polymerization. These disparities provide an interesting target for further expansions of the current *Synechocystis* metabolic reconstructions.

On the other hand, since the number of blocked reactions in *iSyn811* were reported (21), we also decided to identify blocked reactions in *iJN678* in order to compare the connectivity in both models (Dataset S1). *iSyn811* includes a higher number of reactions than *iJN678* (956 versus 863, table S2). However, while the number of blocked reactions in *iSyn811* ranges between 377 and 394 under auto and heterotrophic conditions, respectively only 182 and 188 blocked reaction were found in *iJN678* under the same conditions (Dataset S1). In addition, many of blocked reactions in *iJN678* are involved in alternative carbon and nitrogen sources, which carry flux when the appropriate carbon or nitrogen source is present in the simulation. In fact, there are only 125 blocked reactions (15.5%) in *iJN678* when all the possible carbon and nitrogen source are included in the simulation (Table S1). This indicates that while our reconstruction has a lower number of reactions, it exhibits more connectivity and a higher number of active reactions.

Subsystems	54
Reactions	863
Metabolic reactions	706
Transport reactions	109
Orphan reactions (% of network)	127 (14%)
Exchange reactions	48
^f Blocked reactions (% of network)	125 (14%)
Metabolites	795
Total genes in <i>Synechocystis</i>	3725
Genes (% of genome)	678 (18%)
Number of references included	248
% reactions with reference associated	57%
^a SKI value	0.70

Table S1. Characteristics of the reconstructed metabolic network of *Synechocystis*. ^fBlocked reactions were computed by leaving all the exchange reactions unconstrained (lower/upper bounds of $\pm 10^3$ mmol/gDW/h). ^aSpecies Knowledge Index (SKI) was calculated as described in (34).

Model Name	Genes	Reactions	Metabolites	^a BOF Level	Photosynthesis Modeling	Lipid Modeling	Complete Mass /Charge Balancing	Compartments	Reference
<i>iJN678</i>	678	863	795	Advance	Complete	Complete	Yes	[e],[p],[c],[u]	This study
-	Nd	93	Nd	Basic	Lumped	No	No	[e],[c]	(18)
-	78	56	72	Basic	Lumped	No	No	[e],[c]	(35)
-	505	652	701	Basic	Lumped	No	No	[e],[c]	(19)
-	Nd	46	29	Basic	Lumped	No	No	[e],[c]	(36)
-	343	380	291	Intermediate	Lumped	^d Partial	No	[e],[c]	(20)
<i>iSyn669</i>	^b 669	882	790	Intermediate	^c Complete	^d Partial	No	[e],[c]	(22)
<i>iSyn811</i>	881	956	911	Intermediate	^c Complete	^d Partial	No	[e],[c]	(21)

Table S2. Comparison of *iJN678* with previous metabolic reconstructions from *Synechocystis*. ^aBOF level definition was taken from (33). ^bOnly 589 genes were found in the Additional File 1: ‘iSyn669 reactions to gene connections’ (22). ^c*iSyn669* and *iSyn811* lack of key photosynthetic pathways such as MEHLER and PHOTOR, well-compartmentalized photosynthetic modeling and the interaction between respiration and photosynthesis is not captured. ^d These models include fatty acid biosynthesis pathways but they lack of phospho- and photosynthetic-specific lipids modeling. Compartments symbols were taken from (14). [e] extracellular space; [p] periplasm; [c] cytoplasm; [u] thylakoid.

2. *i*JN678 represents a database of current biochemical, genetic and genomic (BiGG) knowledge about *Synechocystis*

A confidence score was assigned to each reaction in the network on the basis of available experimental evidence. *i*JN678 therefore represents a comprehensive knowledge base that summarizes and categorizes the information currently available for *Synechocystis*. On completion, the reconstruction had an overall average confidence score of 2.87. In fact, 57% of the metabolic reactions in *Synechocystis* included in *i*JN678 have been very well or well-studied, while 43% were primarily based on the genome annotation. A heat map depicting the experimental evidence available for the different subsystems is shown in Fig. S3. This categorization allowed us not only to identify well-known metabolic pathways in *Synechocystis*, but also to identify those pathways that are poorly understood. Future research efforts should be directed towards this latter group. In this sense, the current knowledge reflects the traditional use of *Synechocystis* as a photosynthetic-model bacterium and subsystems such as the photosynthetic pathways and the biosynthesis of photosynthesis pigments are well studied. In contrast, the *Synechocystis* subsystems involved in cofactor biosynthesis, such as riboflavin, vitamin B6, thiamine, pantothenate, biotin and folate, along with the subsystems involved in the synthesis of amino acids and nucleotides, are in need of further characterization (Fig. S3).

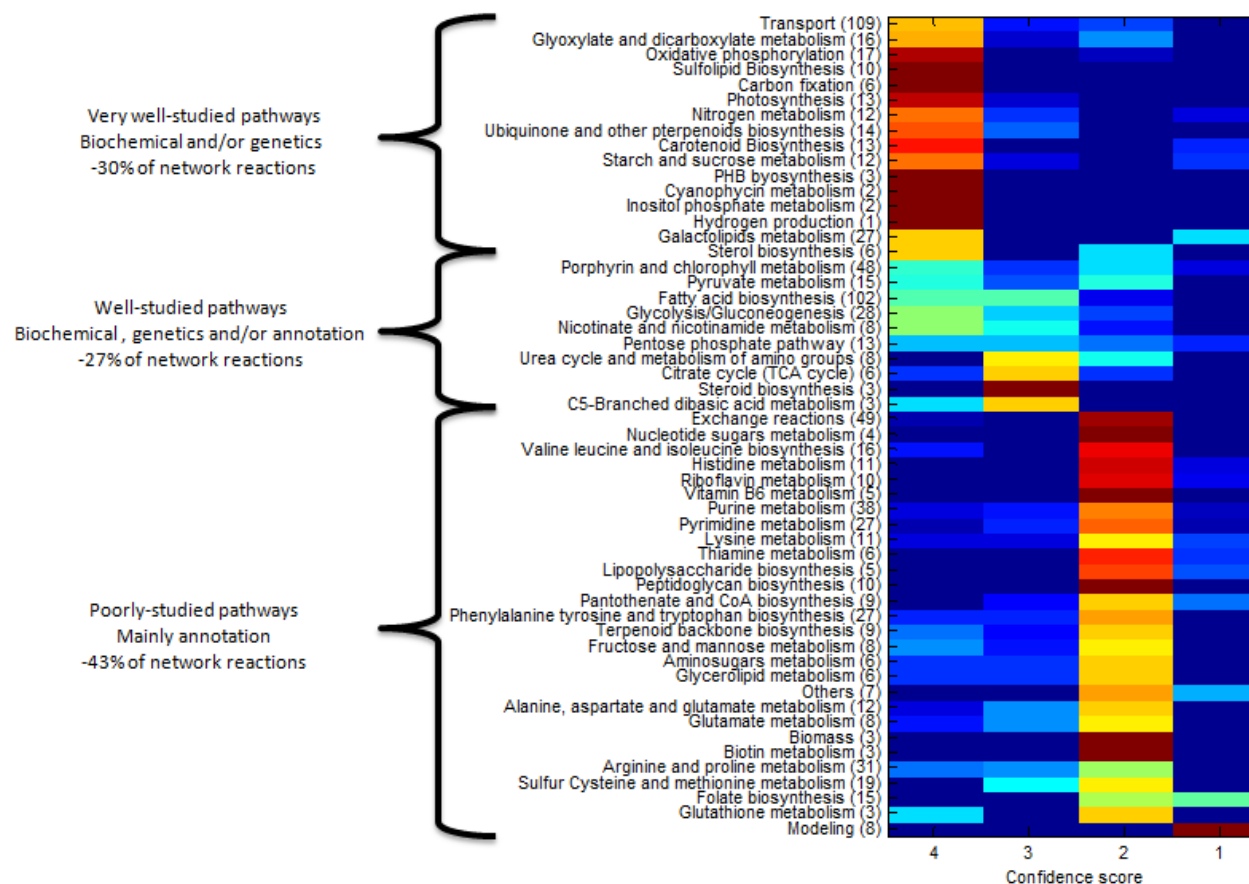


Figure S3. A comprehensive knowledge base that summarizes and categorizes the information currently available for *Synechocystis*. Subsystems and number of reactions in each subsystem are listed. The various colors correspond to the percentage of subsystems reactions that have the corresponding confidence score (red = 100%, blue = 0%). The confidence level was based on a scale from 1 to 4. A score of 4 was assigned when are available direct experimental evidence for gene product function and biochemical reaction; 3 represents physiological, genetic, or proteomic evidence; 2 corresponds to only genome annotation evidence for a gene product and its reaction(s); and finally a score of 1 reflects that no evidence is available, but the reaction is required for modeling functionality (e.g., production of biomass precursor).

3. Computation of the *Synechocystis* growth rate

Comparisons of *in silico* growth rates with experimental data are valuable in network evaluation. The growth capability of *iJN678* in BG-11 *in silico* medium (*i*BG-11) (see Supplementary Methods) under autotrophic, mixotrophic and heterotrophic conditions was determined by using flux balance analysis (FBA) and experimentally determined carbon uptake rate as constraints (Table S3). Under heterotrophic conditions at the expense of glucose as the sole carbon and energy source, *iJN678* exhibited a slightly lower growth rate than the experimental reported values (0.063 h^{-1} vs 0.076 h^{-1}), (37). In addition, Yang et al reported an interesting mixotrophic culture condition in which atmospheric CO_2 was removed and,

consequently, only intracellular CO₂ was available. By simulating these conditions, *iJN678* exhibited a growth rate that was practically identical to the experimental values (Table S3). This agreement is only one example of the predictive potential of the COBRA approach and it shows how the *in silico* predictions can become precise by using additional constraints. Autotrophic conditions were simulated by constraining the CO₂ uptake rate to -3.7 mmol.gDW⁻¹.h⁻¹ (18) while the light uptake rate remained unconstrained. The growth rate was a function of the light and availability of CO₂ under these conditions (Fig S4). The predicted phototrophic maximal growth rate was almost identical to the experimentally reported growth rate (18, 38) (Table S3). The photosynthetic quotient defined as moles of O₂ released per mole of CO₂ fixed was estimated as 1.51. This value falls within the observed range for several photosynthetic organisms (18, 39). The minimum photon uptake rate necessary for maximal growth was calculated to be 54.5 mmol.gDW⁻¹.h⁻¹. Taking the typical mass and diameter of a *Synechocystis* cell, 0.5 pg and 1.75 μm respectively (18), and assuming the maximal efficiency of photosynthesis to be 4.6 - 6% (40), the optimal photon uptake translates to a irradiance of approximately 13.14 - 17.14 μE.m².s⁻¹ which is close to the minimum light intensity required for optimal growth of *Synechocystis* and other cyanobacteria, 15 - 75 μE.m².s⁻¹ (41).

Culture		Growth rate μ (h ⁻¹)	Glucose uptake q_{glc} (mmol/g _{DW} /h)	O ₂ evolution q_{O_2} (mmol/g _{DW} /h)	CO ₂ evolution q_{CO_2} (mmol/g _{DW} /h)
Heterotrophic	<i>Synechocystis</i> ⁽³⁷⁾	0.076	0.85	Nd	1.99
	<i>iJN678</i>	0.063	<u>0.85</u>	(-)1.18	2.53
Mixotrophic	<i>Synechocystis</i> ⁽³⁷⁾	0.059	0.38	Nd	0.0
	<i>iJN678</i>	0.056	<u>0.38</u>	1.19	^a <u>0.0</u>
Autotrophic	<i>Synechocystis</i> ⁽¹⁸⁾	0.085	0.0	4.82	(-) 3.7
	<i>iJN678</i>	0.088	<u>0.0</u>	5.58	(-) <u>3.7</u>

Table S3. Comparison of growth rates of the *in silico* strain *iJN678* and *Synechocystis*. Environmental constraints applied in the simulations are underlined. ^aCi uptake was not allowed according to the mixotrophic conditions reported by Yang et al (37).

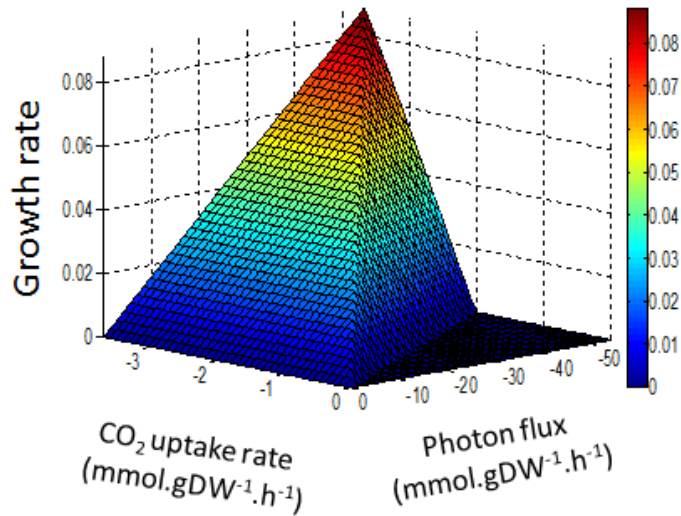


Figure S4. *Synechocystis*' growth under autotrophic conditions as a function of photon and CO₂ uptake.

4. Internal flux distributions: prediction and validation

Metabolic flux analysis (MFA) is a powerful tool for understanding CO₂ fixation and light-energy utilization of photosynthetic organisms during photoautotrophic cultivation. However, techniques for experimental measurement of system-wide metabolic fluxes in purely photoautotrophic systems (using CO₂ as the sole carbon source) have not yet been well developed and metabolic flux quantification in photosynthetic organisms is difficult to perform on a systemic level. Consequently, the metabolic flux distribution in photosynthetic organisms remains poorly understood (42). The *in silico* flux distributions corresponding to maximum growth were obtained by maximizing the biomass objective function. Comparisons with experimental flux values are not only a useful tool for validating the model but also for the generation of new hypotheses.

In heterotrophic growth conditions, glucose was funneled mainly through the oxidative pentose phosphate (OPP) pathway, followed by the NAD-dependent glyceraldehyde-3-phosphate dehydrogenase (GAP1), which drives the carbon flux to the incomplete TCA cycle (Fig. S5, Dataset S3). Our results were in good agreement with previous experimental data (37, 43, 44) ($\tau = 0.89$), and computational predictions (18, 20, 35). The high flux through the OPP, glucose 6-phosphate dehydrogenase (G6PDH) and phosphogluconate dehydrogenase (GND) and the flux across GAP1, as well as the significant flux across the TCA cycle (mainly the NADPH-dependent isocitrate dehydrogenase) provides reducing power in the form of NAD(P)H. In

addition, the TCA cycle supplied important biosynthetic precursors together with carbon skeletons for nitrogen fixation in the form of 2-oxoglutarate (Fig. S5). Interestingly, our *in silico* analysis suggested that succinate was generated through the GABA shunt (Fig. S5), while the succinate semialdehyde dehydrogenase (SSALyr) further increased the NADPH levels. Finally, the reducing power was oxidized by the NADPH and SDH dehydrogenase complexes, contributing to energy production under heterotrophic conditions which supports previous reports (1, 30) (Fig. S5).

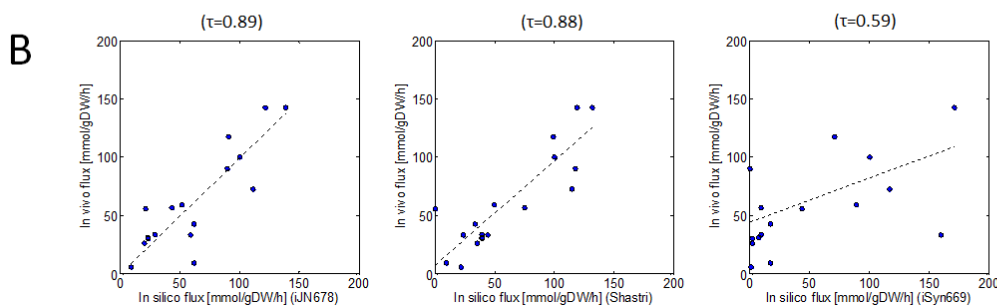
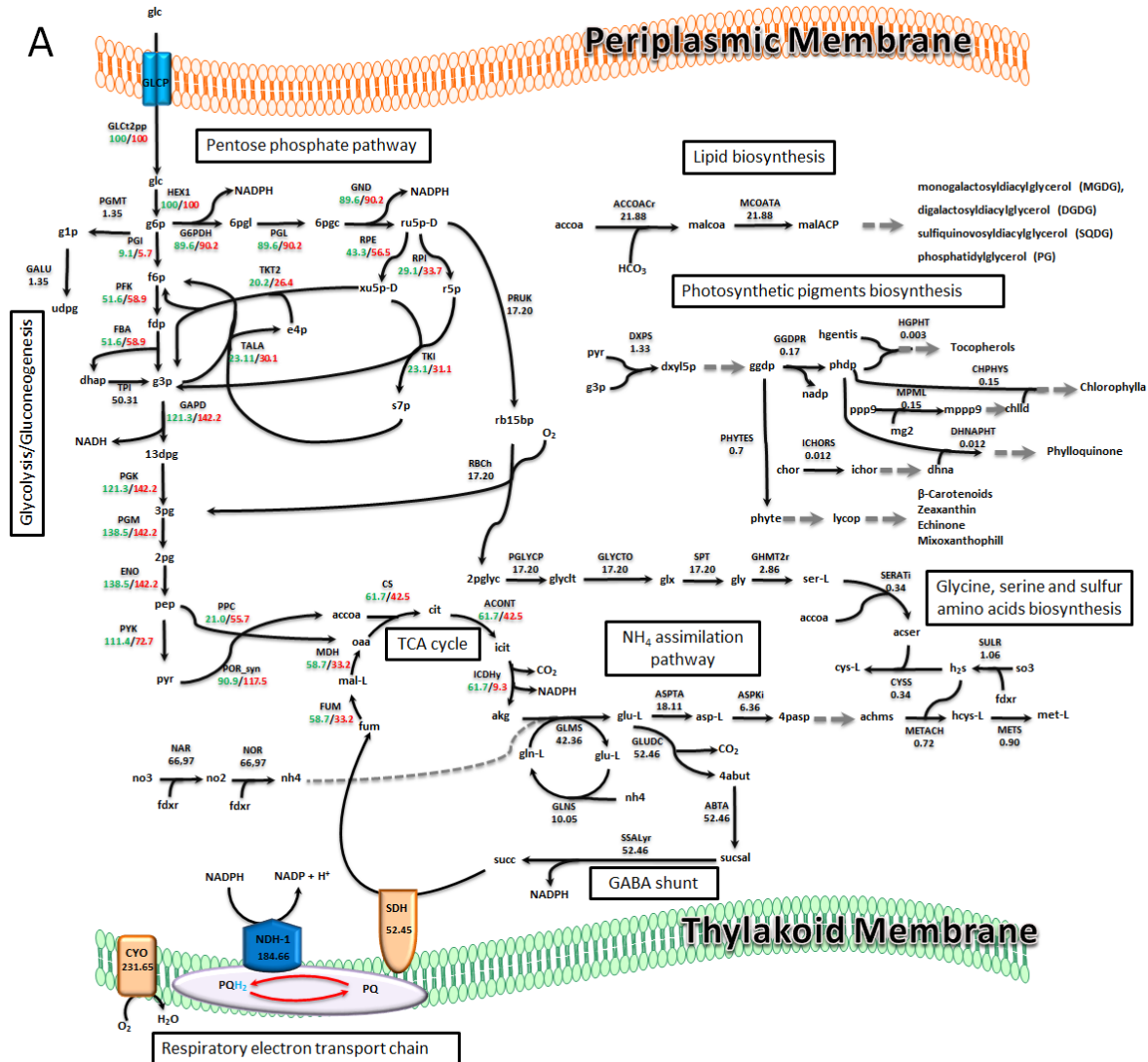


Figure S5. Flux distribution predicted under heterotrophic conditions. (A) Predicted flux values (green) compared with the experimental flux values (red) reported by Yang et al (37) under heterotrophic conditions. Values in black represent *in silico* flux predictions for which no experimental data are available. The net fluxes were normalized to the glucose uptake rate, which was 0.85 mmol/gDW/h. Metabolic pathways involved in the central, nitrogen, and sulfur metabolisms as well as those modeled for first time in *iJN678* are shown in black boxes. Arrows indicate the direction of the estimated fluxes. The flux distribution was obtained by FBA. (B) *In vivo* and *in silico* flux values correlation expressed as Kendall's rank correlation coefficient (τ) for *iJN678*, the central metabolism reconstruction from Shastri and Morgan (18) and *iSyn699* (22).

Under autotrophic conditions, the photosynthetic apparatus generates the reducing power and produces ATP. The flux map obtained under these conditions therefore reveals a completely different carbon-flux distribution compared to heterotrophic conditions (Fig. S6, Dataset S3). The RuBisCO provided 3-phosphoglycerate (3PG), which was split towards the TCA cycle, led by the phosphoglycerate mutase (PGM) and the Calvin cycle, and driven by the phosphoglycerate kinase (PGK). The PGM / PGK ratio of 1/7.6 is slightly higher than the textbook ratio of 1/5 due to the demand of precursors for biosynthesis but is close to previous computational estimations (18, 20). In contrast to the heterotrophic flux distribution, we found that the production of pyruvate under autotrophic conditions relied mostly on the NADP⁺-dependent malic enzyme (ME1) and not from pyruvate kinase (PYK) (Fig. S5-6). This data, although in contrast with the previous computational flux predictions (18), has been recently validated by in vivo flux distribution data (45), and is in good agreement with an experimental study where the pyruvate pathway was found to involve phosphoenolpyruvate carboxylase (PPC), malate dehydrogenase (MDH) and ME1 (29). The calculated flux distribution was also consistent i) with the observation that *cyanobacteria* can convert significant amounts of CO₂ into malate in light conditions (46) and ii) with the properties of a C₄-like photosynthetic metabolism through phosphoenolpyruvate synthase (PPS) and ME1, which has been described for *cyanobacteria* (37).

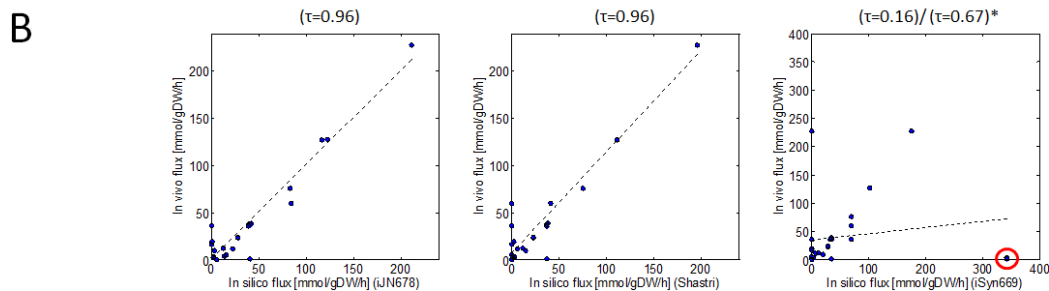
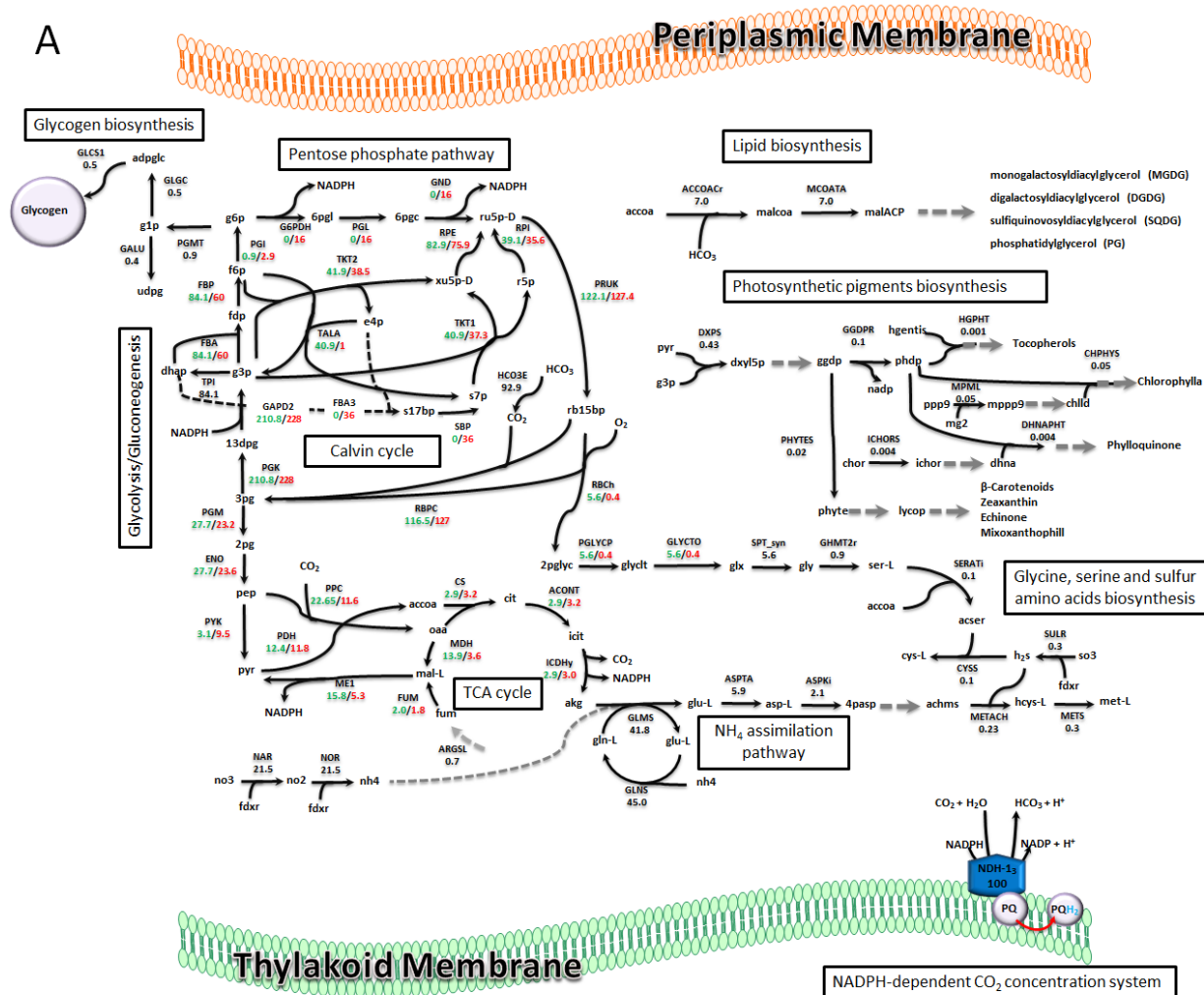


Figure S6. Flux distribution predicted under autotrophic conditions. (A) Predicted flux values (green) compared with the previous flux values predictions (red) reported under autotrophic conditions (45). Values in black represent *in silico* flux predictions for those reactions for which no experimental data have been reported. The net fluxes were normalized to the CO₂ uptake rate, which was 3.7 mmol/gDW/h. Metabolic pathways involved in the central, nitrogen, and sulfur metabolisms as well as those modeled for first time in *iJN678* are shown in black boxes. Arrows indicate the direction of the estimated fluxes. The flux distribution was obtained by FBA. (B) *In vivo* and *in silico* flux values correlation expressed as Kendall's rank correlation coefficient (τ) for *iJN678*, central metabolism reconstruction from Shastri and Morgan (18) and *iSyn669* (22).*(τ) value excluding malate dehydrogenase and fumarase (red circle) for *iSyn669*.

On the other hand, the oxygenic activity of the RuBisCO was found to represent 4.5% of the total RuBisCO activity, an estimated value that agrees well with early reported data (4-5%) (20). In addition, the 2-phosphoglycolate that was produced was a key intermediate in the synthesis of glycine, serine and cysteine (Fig.S6). Because no significant fluxes through the GABA shunt or SDH were predicted in our analysis, the optimal flux distribution around the TCA cycle therefore reflects an incomplete TCA cycle in which fumarate was mainly synthesized from arginine.

Under mixotrophic conditions, glucose was metabolized via the non-oxidative pentose phosphate pathway to produce ribulose-1,5-diphosphate. Furthermore, 3PG was produced by RuBisCO and followed the same flux distribution as described above for the autotrophic condition (Fig S7, Dataset S3). However, the PGM/PGK ratio was reversed under mixotrophic conditions due to the flux of exogenous glucose to fructose-6-phosphate. Pyruvate was mainly produced by PYK. Another interesting characteristic of the mixotrophic metabolism was that a small but significant respiratory rate is predicted for maximum growth under this condition. Overall, these results provide evidence, as was expected, for the concurrence of both autotrophic and heterotrophic metabolism under mixotrophic conditions (Fig. S7, Dataset S3).

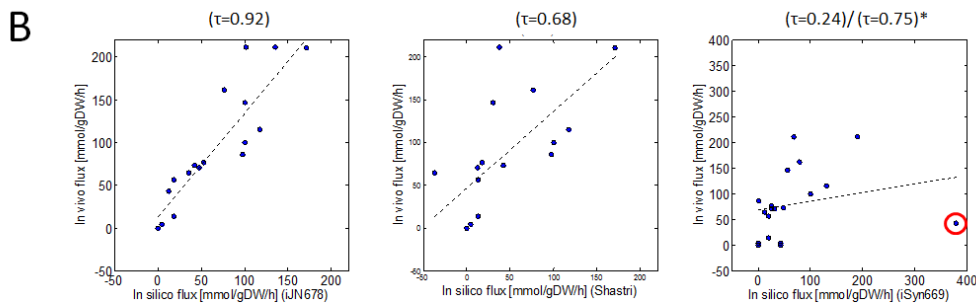
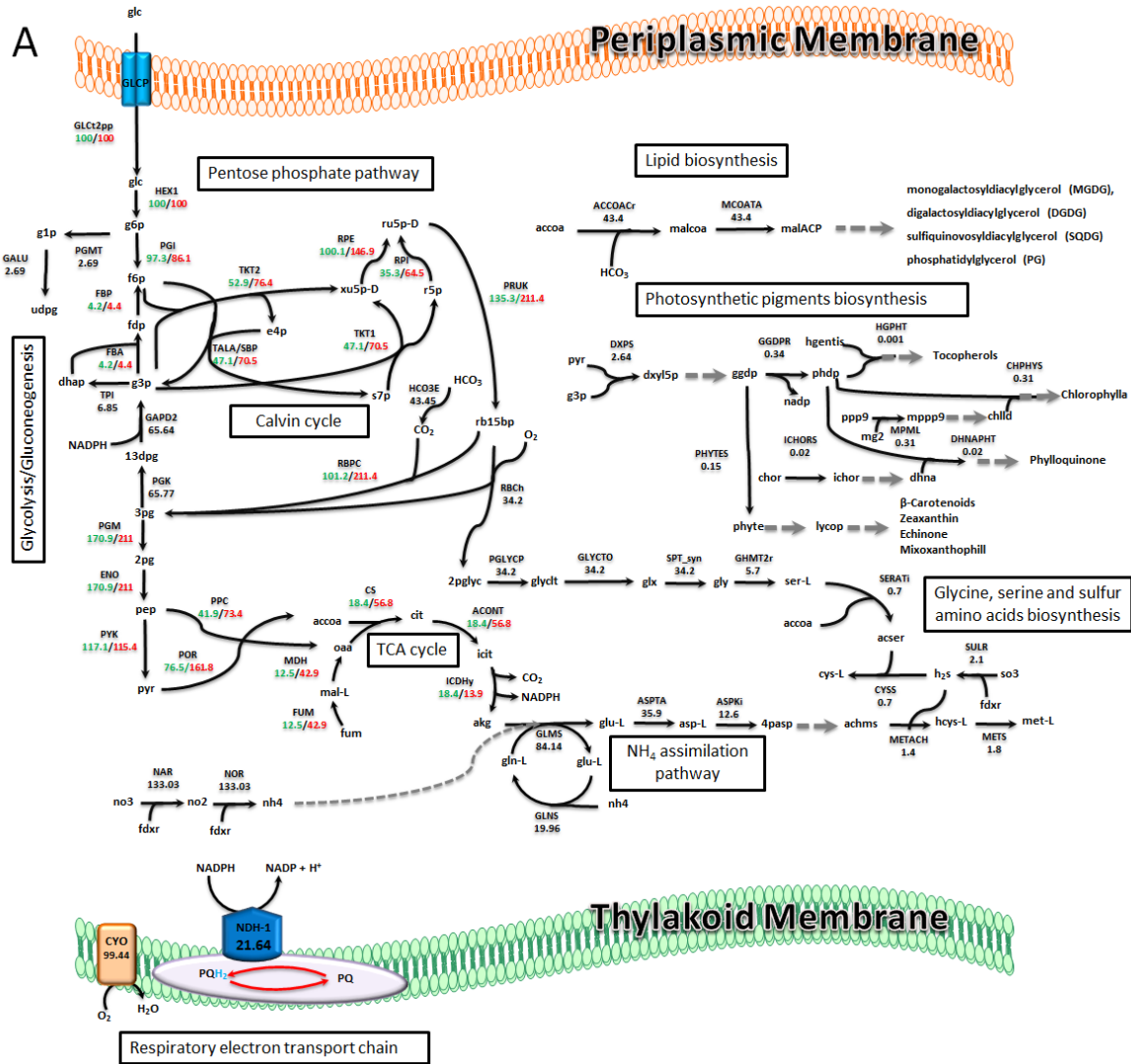


Figure S7. Flux distribution predicted under mixotrophic conditions. (A) Predicted flux values (green) compared with the experimental flux values (red) reported by Yang et al (37) under mixotrophic conditions. Values in black represent *in silico* flux predictions for those reactions for which no experimental data have been reported. The net fluxes were normalized to the glucose uptake rate, which was 0.38 mmol/gDW/h, no CO₂ uptake was allowed in the simulation following the culture conditions used by Yang et al. Metabolic pathways involved in the central, nitrogen, and sulfur metabolisms as well as those modeled for first time in *iJN678* are shown in black boxes. Arrows indicate the direction of the estimated fluxes. The flux distribution was obtained by FBA. **(B)** *In vivo* and *in silico* flux values correlation expressed as Kendall's rank correlation coefficient (τ) for *iJN678*, central metabolism reconstruction from Shastri (18) and *iSyn699* (22).* (τ) value excluding malate dehydrogenase and fumarase (red circle) for *iSyn699*.

The correlation between the *in vivo* flux distribution data and those estimated *in silico* with *iJN678*, *iSyn669* and the central metabolism reconstruction from Shastri and Morgan was estimated using Kendall's rank correlation coefficient in order to estimate the accuracy of our flux distribution predictions. *iSyn669* was selected because it was used in an exhaustive flux distribution analysis under various culture conditions (22). The reconstruction of Shastri and Morgan was selected because it was the first metabolic reconstruction published and because this model has been used for computing *in vivo* flux distribution data under autotrophic conditions (45). We found that the flux distribution estimated with *iJN678* correlated well with *in vivo* flux distributions under hetero, mixo and autotrophic conditions ($\tau = 0.89, 0.92$ and 0.96 respectively) (Fig. S5-7). The prediction accuracy of *iJN678* was slightly higher than for the Shastri reconstruction, but significantly higher than for *iSyn669*. *iSyn669* was able predict flux distribution under heterotrophic conditions with moderate accuracy, but failed to predict flux distribution under mixotrophic and autotrophic conditions. The modeling of the glucose metabolism under heterotrophic conditions has been well established and numerous metabolic reconstructions include it. The autotrophic metabolism is however, still under development. The high prediction accuracy found in *iJN678* highlights the detailed modeling of the autotrophic metabolism found in our reconstruction and makes *iJN678* a template reconstruction for further genome-scale reconstruction of photosynthetic bacteria.

5. Study of the proton flux exchange in *Synechocystis*

Changes in environmental conditions, such as temperature, pH, osmolarity, carbon source and electron donors, affect the internal pH as well as energy generation. The cells have to regulate the internal pH by secreting or consuming protons in order to maintain energy homeostasis. The estimation of proton secretion and consumption associated with both cellular growth and metabolism can provide new insights into the metabolism of the target microorganism and can be used to further validate the model. In order to study the proton flux exchange in *Synechocystis*, the growth rate under autotrophic (using CO_2 and HCO_3^- as *Ci* source, autotrophic _{CO_2} and autotrophic _{HCO_3^-} respectively), mixotrophic and heterotrophic conditions was computed as a function of the proton flux exchange (Fig. S8). Our analysis revealed that the growth rate was strongly dependent on active proton uptake in all the conditions tested. While

the mixotrophic and autotrophic_{CO₂} conditions were slightly more sensitive to proton exchange compared to the heterotrophic condition, the predicted growth rates exhibited similar behavior, suggesting that light availability and photosynthetic activity have a modest impact on proton exchange (Fig. S8). Under autotrophic_{HCO₃⁻} conditions, proton uptake was found to be strictly necessary for growth and higher medium alkalization was predicted (Fig. S8). Interestingly, the predicted proton uptake and subsequent medium alkalization were in agreement with the basic medium reported in *Synechocystis* cultures grown under autotrophic conditions (up to pH 10.9) (9, 47). The key reason is that the H⁺ consumed in the conversion of HCO₃⁻ to CO₂ in the carboxysome by carbonic anhydrase leads to an accumulation of OH⁻ inside the cell that will need to be neutralized by H⁺ uptake from the external medium (9). In summary, our analysis is an example of how both the internal proton balancing and the external pH can be predicted by using a completely mass and charge balanced model. In addition, our data highlights that the main factor that drives the proton exchange mechanism in a photosynthetic organism is the carbon source rather than the light availability. The former observation has previously been made for other non-photosynthetic organisms (48).

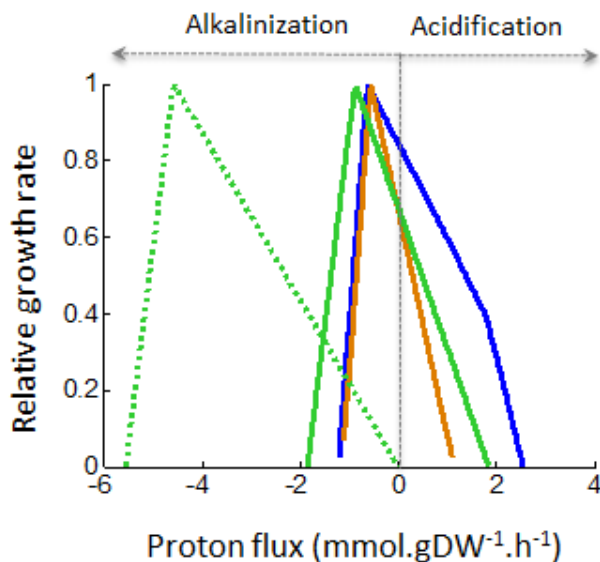


Figure S8. Effect of proton exchange on predicted growth rate. The exchange of protons between the cell and the medium was varied from -6 to 4 mmol.gDW⁻¹.h⁻¹ and the relative growth rate was computed under heterotrophic (blue line), mixotrophic (orange line) and autotrophic conditions, using CO₂ (green solid line) and HCO₃⁻ (green dots line) as inorganic carbon, respectively.

6. Metabolic robustness and gene essentiality study of *iJN678*

We studied the minimum number of genes required to sustain growth under autotrophic, mixotrophic and heterotrophic conditions by using gene essentiality analysis (see Supplementary Methods (49, 50)). While 350 genes were found to be essential in the autotrophic condition, significantly fewer genes were predicted to be essential in the heterotrophic and mixotrophic conditions: 261 and 259 respectively (Fig S9A). A core of 259 genes was predicted to be essential in all of the conditions, while 91 genes were predicted to be essential only under autotrophic conditions, and two genes only under heterotrophic conditions (Fig. S9B). Genes mainly involved in the biosynthesis of lipids, amino acids, photosynthetic pigments, purines and pyridines, as well as other biosynthetic pathways, were predicted to be lethal in all conditions (Dataset S5). In the absence of a systematic gene essentiality analysis in *Synechocystis*, we used the *Synechocystis* mutant collection available in cyanomutant (51) (<http://genome.kazusa.or.jp/cyanobase/mutants/>) to validate our predictions. A total of 190 genes included in *iJN678* are present in cyanomutant, of which 44 and 41 have been predicted as essential and non-essential genes respectively (Fig. S9C, Dataset S5). Excluding mutants for which non-specific phenotype has been reported; our gene essentiality analysis correctly predicts 79% of the phenotypes described in Cyanomutant (two-sided p-value of Fisher's exact test is less than 10^{-3}). However, we found a significant false positive rate (21%). These are genes that are predicted as essential *in silico* but are non-essential *in vivo* (Fig. S9C). Many of these false positives were imposed by detailed biomass objective functions, which require the synthesis of several photosynthetic pigments and lipids. For example, the gene *slr008*, which encodes for a β -carotene ketolase involved in the synthesis of echinenone, was predicted to be essential. Yet this mutant strain was unable to synthesize echinenone, a metabolite included in our BOF reactions, and its cell viability was not compromised *in vivo* (52), which strongly suggests a high flexibility in the composition of photosynthetic pigments in *Synechocystis* (53). Another group of false positives included genes that were involved in the uptake of metal ions. This suggests that alternative metal transport systems may be present in *Synechocystis* and is in agreement with the high number of putative metal and ion-transporter systems encoded in its genome (Fig. S2). These disparities provide an interesting target for knowledge discovery in the role of photosynthetic pigments as well the metal uptake systems in *Synechocystis*.

Only two genes were found to be essential in the heterotrophic condition (Fig. S9B, Dataset S5): *glcP* (sll0771) and *glk* (sll0593). These genes are involved in the first two steps of glucose metabolism, i.e., glucose transport across the inner membrane and its subsequent phosphorylation, producing glucose-6-phosphate. Interestingly, these two genes were reported as essential *in vivo* under the same conditions (27, 54).

On the other hand, most of the 91 essential genes in *Synechocystis* found under autotrophic conditions (Dataset S5) were involved in the photosynthetic machinery, which is in agreement with previous reports (55, 56). In addition, other essential genes were found in the non-oxidative branch of pentose phosphate pathway (Calvin cycle). It is important to note that while glucose is funneled to the pentose phosphate pathway, deletion of genes such as *rpe* (sll0807), *tpi* (sll0783) and *pgk* (slr0394) were only predicted to be lethal under autotrophic conditions. Synthetic lethality has been used as a measure of the robustness of metabolic networks (57). It is associated with gene products, which i) are interchangeable (isoenzymes), ii) act in the same essential pathway, or iii) operate in separate pathways with redundant and/or complementary essential functions. According with the essential genes analysis, a higher number of synthetic lethal genes were predicted under heterotrophic conditions, 234 against only 158 synthetic lethal genes predicted under autotrophic conditions. (Fig. S9A). Taken together, these results suggest reduced metabolic robustness under genetic perturbations in *Synechocystis*, especially under autotrophic conditions.

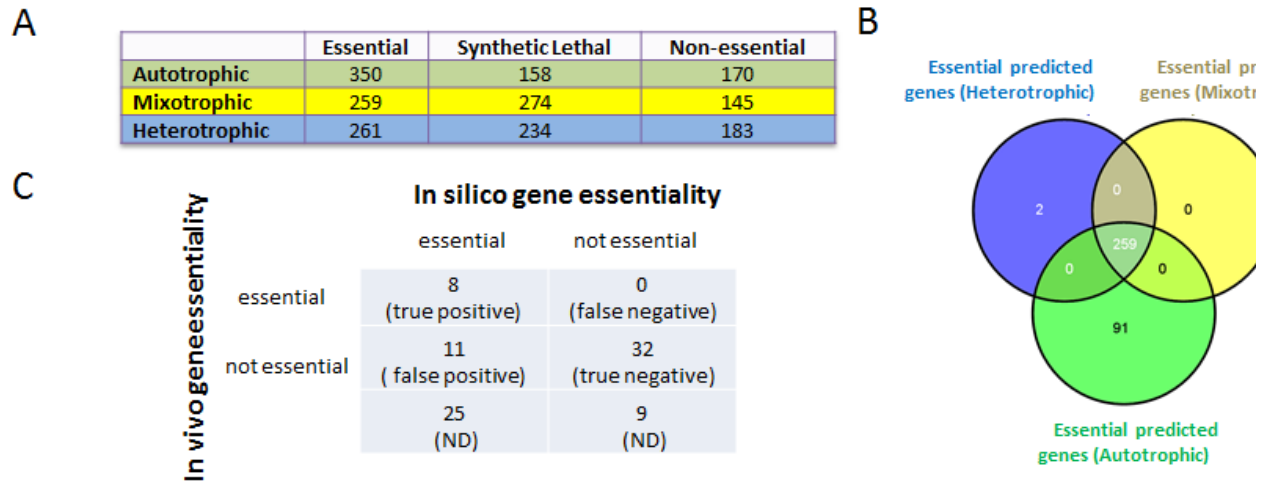


Figure S9. Gene essentiality and synthetic lethality analysis of *Synechocystis*. (A) Essentiality and synthetic lethality analysis in the different growth conditions. (B) Comparison of essential genes under heterotrophic (blue), mixotrophic (yellow) and autotrophic (green) conditions. Venn diagrams were generated by using Venny (58). (C) *In vivo/in silico* comparison of the core essential and non-essential genes. ND represents those knock-outs included in Cyanomutant but with unknown phenotype or segregation state.

7. Analysis of the heterotrophic metabolism of *Synechocystis*

The analysis of the genes encoding for transporters suggested that the hetero- and mixotrophic metabolisms have a more important role in *Synechocystis* than previously thought (Fig. S2). The culture of photosynthetic organism under mixo- and heterotrophic conditions have many advantages organisms amount others, higher efficiency and lower cost in conventional microbial fermenters (59). This fact led us to carry out an extensive analysis of the hetero- and mixotrophic metabolisms of *Synechocystis*. Thus, we tested each metabolite that has an associated transport reaction as carbon and nitrogen sources in presence of light (mixotrophic) and in the dark (heterotrophic) (Table S4). The growth predictions suggest a broader heterotrophic metabolism than we expected for a facultative heterotrophic microorganism. *iJN678* was able to grow heterotrophically on several organic compounds besides glucose, including fructose, pyruvate, acetate, fumarate, succinate, citrate, oxoglutarate and malate (Table. S4). In addition, some amino acids such as alanine, glutamine and serine under mixotrophic conditions, together with glutamate under both mixo- and heterotrophic conditions, completed the list predicted carbon sources. It is well known that *Synechocystis* is able to use several organic compounds as nitrogen sources instead of nitrate or ammonium (23). Our analysis confirmed that arginine, urea and cyanate were efficient nitrogen sources. In addition, several other amino acids such as alanine, glycine, glutamate, glutamine and serine were predicted here as potential nitrogen sources for *Synechocystis* (Table S4).

Carbon source	Nitrogen source
---------------	-----------------

Metabolite	Mixotrophic (<i>In silico</i> / <i>In vivo</i>)	Chemoheterotrophy (<i>In silico</i> / <i>In vivo</i>)	Mixotrophic (<i>In silico</i> / <i>In vivo</i>)	Chemoheterotrophy (<i>In silico</i> / <i>In vivo</i>)
Glucose	(+/+) ⁽⁶⁰⁾	(+/+) ⁽⁶⁰⁾	(-/-)	(-/-)
Fructose	(+/ \pm) ^(60, 61)	(+/ \pm) ^(60, 61)	(-/-)	(-/-)
Acetate	(+/+) ⁽²⁸⁾	(+/+) ⁽²⁸⁾	(-/-)	(-/-)
Fumarate	(+ND)	(+ND)	(-/-)	(-/-)
Succinate	(+ND)	(+ND)	(-/-)	(-/-)
Citrate	(+/+) ⁽²⁸⁾	(+/+) ⁽²⁸⁾	(-/-)	(-/-)
Oxoglutarate	(+ND)	(+ND)	(-/-)	(-/-)
Malate	(+/+) ⁽²⁸⁾	(+/+) ⁽²⁸⁾	(-/-)	(-/-)
Pyruvate	(+/+) ^(28, 29)	(+/ \pm) ^(28, 29)	(-/-)	(-/-)
Alanine	(+ND)	(-ND)	(+ND)	(+ND)
Arginine	(-/-) ⁽²³⁾	(-/-) ⁽²³⁾	(+/+) ⁽²³⁾	(+/+) ⁽²³⁾
Glycine	(-/-) ⁽²³⁾	(-/-) ⁽²³⁾	(+ND)	(+ND)
Glutamate	(+ND)	(+ND)	(+/+) ⁽²³⁾	(+ND)
Glutamine	(+ND)	(-ND)	(+/+) ⁽²³⁾	(+ND)
Histidine	(-ND)	(-ND)	(-/-) ⁽²³⁾	(-/-) ⁽²³⁾
Leucine	(-ND)	(-ND)	(-/-) ⁽²³⁾	(-/-) ⁽²³⁾
Lysine	(-ND)	(-ND)	(-/-) ⁽²³⁾	(-/-) ⁽²³⁾
Proline	(-ND)	(-ND)	(-/-) ⁽²³⁾	(-/-) ⁽²³⁾
Serine	(+ND)	(-ND)	(+ND)	(+ND)
NO ₃ ²⁻	(-/-)	(-/-)	(+/+) ⁽²³⁾	(+/+) ⁽²³⁾
NH ₄ ⁺	(-/-)	(-/-)	(+/+) ⁽²³⁾	(+/+) ⁽²³⁾
Urea	(-/-)	(-/-)	(+/+) ⁽²³⁾	(+/+) ⁽²³⁾
Putrescine	(-/-) ^(62, 63)	(-/-) ^(62, 63)	(-/-) ^(62, 63)	(-/-) ^(62, 63)
Spermidine	(-/-) ^(62, 63)	(-/-) ^(62, 63)	(-/-) ^(62, 63)	(-/-) ^(62, 63)
Cyanate	(-/-)	(-/-)	(+/+) ⁽²³⁾	(+/+) ⁽²³⁾
Glucosylglycerol	(-/-) ^(64, 65)	(-/-) ^(64, 65)	(-/-)	(-/-)
Sucrose	(-/-) ^(64, 65)	(-/-) ^(64, 65)	(-/-)	(-/-)

Table S4. Comparisons of *in silico* growth predictions and *in vivo* experimental data. (+) growth predicted / growth experimentally reported. (-) no growth predicted / no growth experimentally reported. (\pm) contradictory experimental reports found. ND condition not tested experimentally. Experimental references are indicates.

Metabolite	Mixo	Hetero	Metabolite	Mixo	Hetero
------------	------	--------	------------	------	--------

Metabolite	Mixo	Hetero	Metabolite	Mixo	Hetero
Glucose	1	1	L-erythro-4-Hydroxyglutamate	1	0.784
4-Aminobutanal	0.899	1.056	Succinic semialdehyde	1	0.894
4-Aminobutanoate	0.899	0.918	L-Glutamate 5-semialdehyde	1	0.931
Aspartate	0.899	0.422	Galactose	1	1
Glycolaldehyde	1.001	0.972	(R)-Glycerate	1.001	0.853
D-Alanyl-D-alanine	0.599	0	Glycolate	1.001	0.8
D-Glyceraldehyde	1.001	0.981	D-Lactate	1.001	0.885
Glycerol	1.001	1.123	L-1-Pyrroline-3-hydroxy-5-carboxylate	1	0.979
Ethanol	1.001	0.992	Hydroxypyruvate	1.001	0.733
Acetaldehyde	1.001	0.768	D-Lactaldehyde	1.001	0.992
N(omega)-(L-Arginino)succinate	0.36	0.208	Maltose	1	0.999
Oxaloacetate	1	0.586	Methylglyoxal	1.001	0.872
Formate	0.999	0	Ornithine	0.36	0.424
4-Hydroxy-2-oxoglutarate	1	0.714	1-Pyrroline-5-carboxylate	1	0.944
Glyoxylate	1.001	0.564	D-Ribose	1	1
Deoxyribose	1	0.982	Oxalate	1.001	0

Table S5. Potential new carbon sources for *Synechocystis*. For the evaluation of the new carbon sources, a cytoplasmatic sink reaction for each internal metabolite was introduced in the model and the growth rate in the presence (mixotrophic) and absence (heterotrophic) of light was computed. An uptake rate of 1 mmol.gDW⁻¹.h⁻¹ was used. The growth rate relative to glucose is also shown.

In order to complete our analysis regarding the heterotrophic metabolism in *Synechocystis*, we tested the ability of *iJN678* to grow each of the included internal metabolites as sole carbon source under hetero- and mixotrophic conditions (see Supplementary Methods). This approach could lead to the discovery of new carbon sources based on the metabolic capabilities of *Synechocystis* that were included in *iJN678* despite missing transport reactions (e.g., due to missing annotation). 31 new carbon sources were predicted (Table S5), including storage polymers such as aspartate (a cyanophycin derivative); carbohydrates such as maltose, galactose, D-ribose and deoxyribose; organic acid derivatives from the glutamate metabolism, such as succinic semialdehyde, hydroxypyruvate, etc.; as well as other compounds, such as glycerol, glycolate, glyoxylate, and lactate (Table S5).

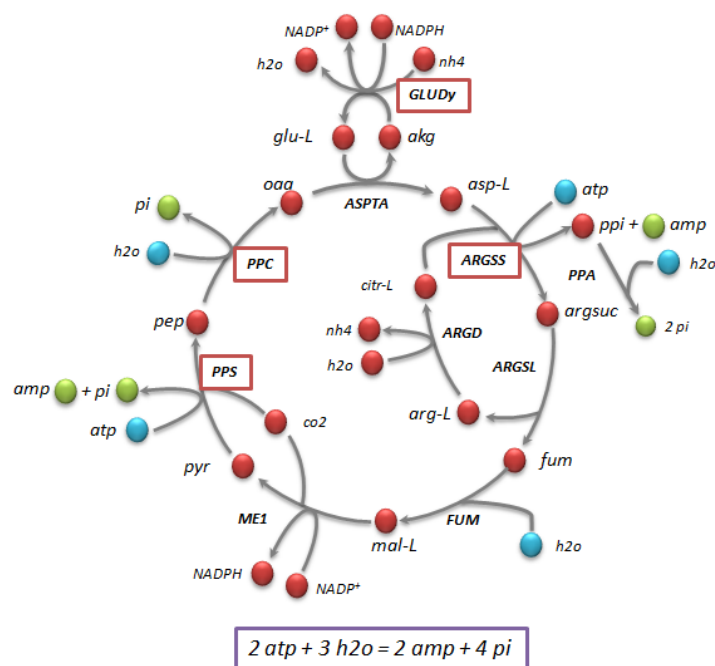


Figure S10. Futile metabolic cycle proposed for ATP/ADP balancing in *Synechocystis* under CLS. Abbreviations for reactions and metabolites are listed in Dataset S1. In red, metabolites produced and consumed. In blue, only metabolites consumed and in green, only metabolites produced. Reactions that have been reported up-regulated under high light and/or low CO₂ are shown in red boxes. The net reaction of the cycle is also indicated.

Supplementary Methods

1. Metabolic reconstruction

The first draft of the *Synechocystis* network was constructed according to the procedure given in Thiele and Palsson (14) and was based on the annotated genome sequence (66) as well as the genomic information available in specific databases, such as Cyanobase (51) and CYORF (<http://cyano.genome.jp/>). Other online databases, e.g., KEGG (67), METACYC (68) and BRENDA (69), were extensively used as well. Finally, we took advantage of previously published metabolic models of *Synechocystis* (18, 19, 35, 36) and of the biochemical information found in cyanobacteria-specific books (70) and general biochemical textbooks. The resulting first draft accounted for the core metabolism of *Synechocystis*, including the Calvin cycle, glycolysis, the incomplete TCA cycle, the pentose-phosphate pathway, amino-acid, nucleotide and cofactor biosynthetic pathways, as well as other minor pathways. The initial draft was subsequently enhanced by including exclusive pathways to define the identity signatures of *Synechocystis*;

thus, a detailed representation of the photosynthetic apparatus, carbon dioxide fixation, synthesis of photosynthetic pigments, specific fatty acids, and storage polymers such as glycogen, cyanophycin and polyhydroxybutyrate were incorporated. A literature search also led to an extension of the initial reactions list, including the recently reported branches of the photorespiration pathway (10) as well as new genes involved in chlorophyll biosynthesis such as slr1790 (71). The network was subject to iterative gap-filling.

The initial analysis revealed incomplete biosynthetic pathways for several amino acids (e.g., glycine, serine, methionine, and cysteine) and cofactors (e.g., thiamine, folic acid). After verification that the respective biosynthetic products can be synthesized by *Synechocystis*, we filled the gaps based on genes present in phylogenetically close organisms. For example, the cysteine biosynthesis pathway was completed using homoserine O-trans-acetylase (EC 2.3.1.31) and O-acetyl-L-homoserine acetate-lyase (EC 2.5.1.49), which are postulated to be present in other cyanobacteria (<http://genome.kazusa.or.jp/cyanobase>). Substrates and cofactors, charged formulas for each metabolite, reaction directionality and stoichiometry, information for gene and reaction localization as well as gene-protein-reaction (GPR) associations for each reaction were carefully revised based on the available information for *Synechocystis* or phylogenetically close cyanobacteria. For instance, the succinate dehydrogenase complex (SDH, EC 1.3.99.1), which is described traditionally as a reversible reaction and FAD-dependent, was included in our reconstruction as an irreversible reaction, plastoquinone (PQ) dependent, and placed both in the thylakoid and cytoplasmic membranes on the basis of experimental data on *Synechocystis* (1, 30). A confidence score was associated with every reaction included in the reconstruction. The score was based on the available evidence for its presence in the *Synechocystis* metabolic network (14). Biochemically characterized enzymes in *Synechocystis* received a confidence score of 4. If genetic knockout information or physiologic evidence was available, a score of 3 was given. A score of 2 was assigned to reactions for which indirect evidence or sequence homology information was available. Multiple types of evidence result in a cumulative confidence score (14). Finally, during gap-filling and evaluation of the network functionality (e.g., biomass precursor production) some reactions were added with a confidence score of 1 (Fig. S3). The complete sets of reactions and metabolites included in the model are given in Dataset S1.

2. Biomass reactions formulation

The biomass reaction accounts for all known biomass constituents and their fractional contribution to the overall cellular biomass (33). A detailed and precise biomass reaction is needed for realistic metabolic network analysis. We formulated the *Synechocystis* biomass reaction according to the procedures given in (14, 33, 72). The fractions corresponding to the main biosynthetic blocks, proteins (51%), carbohydrates (19%), lipids (10%), RNA (17%) and DNA (3%) were based on experimental data (18). The relative fraction of each precursor from protein and nucleic acid blocks was estimated from the genome sequence (14). The relative fraction of each fatty acid was taken from experimental values reported in (16), the composition of glycogen from (73) and the photosynthetic pigments from (53, 74, 75). Finally, the relative fraction of peptidoglycan and soluble pool metabolites was taken from experimental data reported for *Synechocystis* and other Gram-negative bacteria (76, 77).

The energy maintenance, in the form of ATP, for auto-, hetero- and mixotrophic conditions was taken from (18). The relative fraction of growth-associated ATP maintenance reaction (GAM), which accounts for the energy necessary to replicate a cell (e.g., energy required for macromolecular synthesis) and the non-GAM reaction (NGAM), which represents NGAM requirements to maintain other cellular functions (e.g., turgor pressure) was taken from the *E. coli* biomass reaction (72). The phosphate bonds were accounted for by adding ATP hydrolysis to the biomass reaction ($x \text{ ATP} + x \text{ H}_2\text{O} \rightarrow x \text{ ADP} + x \text{ Pi} + x \text{ H}^+$). With the exception of the presence of glycogen in the autotrophic biomass reaction and different energy maintenance requirements (18), the three different biomass reactions for autotrophic, mixotrophic, and heterotrophic conditions have a similar composition. A detailed description of the *iJN678*'s biomass reactions is depicted in Dataset S3.

3. Conversion of the reconstruction into a mathematical model

The conversion of a reconstruction into a mathematical model has been described in detail elsewhere (14). All flux rates, v_i are given in mmol/g_{DW}/h, except biomass formation, which is given in h⁻¹.

4. Analysis of metabolic flux

Numerous mathematical tools have been developed to study metabolic network properties *in silico* (see (78) for a review). Many of the tools rely on (linear) optimization to calculate the property of interest, e.g., the maximal possible growth rate of a metabolic network under a given set of environmental constraints.

In flux balance analysis (FBA) (79), a metabolic network is framed as a linear programming (LP) problem and a specific cellular objective such as the growth rate or substrate secretion is maximized or minimized. The principal sets of constraints in FBA are those imposed by the steady-state mass conservation of metabolites in the system. The LP is formulated as follows:

$$\begin{aligned} & \text{maximize } c^T v \text{ (objective function)} \\ & \text{subject to } S \cdot v = 0 \\ & v_{i,\min} \leq v_i \leq v_{i,\max} \text{ for all } i = 1, \dots, n \text{ reactions,} \end{aligned}$$

where S is the $m \times n$ stoichiometric matrix, c is the objective function vector, v is a vector of reaction fluxes, $v_{i,\max}$ is the maximal capacity for reaction i , and $v_{i,\min}$ is the minimal capacity for reaction i .

Flux variability analysis (FVA) (80) is used to find the minimum and maximum flux for reactions in the network while maintaining some state of the network. FVA requires the solution of $2n$ linear optimization problems, two for each reaction, $i = 1, \dots, n$

$$\begin{aligned} & \max/\min_v v_i \\ & \text{Subject to } S \cdot v = 0 \\ & c^T v \geq \gamma Z_0 \\ & v_{i,\min} \leq v_i \leq v_{i,\max} \end{aligned}$$

where $Z_0 = c^T v_0$ is the optimal solution to the FBA problem above (typically the maximum growth rate) and γ is a parameter that controls whether the analysis is done w.r.t. suboptimal network states ($0 \leq \gamma < 1$) or to the optimal state ($\gamma = 1$). FVA was used in our experiments to find the minimum and maximum flux through each reaction while supporting 99% of the maximal growth rate ($\gamma = 0.99$).

All computational simulations were performed using the COBRA toolbox (81) in the Matlab environment (The MathWorks Inc., Natick, MA). The GNU Linear Programming Kit (GLPK) (<http://www.gnu.org/software/glpk>) and TomLab (Tomlab Optimization Inc., San Diego, CA) were used to solve the linear and quadratic optimization problems respectively.

5. Formulation of *i*BG-11 minimal medium

An *in silico* BG-11 minimal medium was simulated on the basis of the composition of the BG-11 minimal medium routinely used for *Synechocystis* cultures (82), which contains per liter: $\text{CaCl}_2 \cdot 2\text{H}_2\text{O}$ 36 mg; NaNO_3 1.5 g; K_2HPO_4 40 mg; $\text{MgSO}_4 \cdot 7\text{H}_2\text{O}$ 75 mg; $\text{CuSO}_4 \cdot 5\text{H}_2\text{O}$ 0.079 mg; $\text{Na}_2\text{MoO}_4 \cdot 2\text{H}_2\text{O}$ 0.39 mg; H_3BO_3 2.86 mg; $\text{EDTANa} \cdot 2\text{H}_2\text{O}$ 1 mg; NaCO_3 0.02 g; $\text{NH}_4\text{Fe}(\text{C}_6\text{H}_5\text{O}_7)$ 0.006 g; $\text{MnCl}_2 \cdot 4\text{H}_2\text{O}$ 1.81 mg; $\text{ZnSO}_4 \cdot 7\text{H}_2\text{O}$ 0.222 mg; $\text{Co}(\text{NO}_3)_2 \cdot 6\text{H}_2\text{O}$ 0.049 mg. By assuming that these concentrations do not impose a growth restriction, the external metabolites Co^{2+} , Fe^{2+} , Fe^{3+} , H^+ , H_2O , Na^+ , Ni^{2+} , Cu^{2+} , Zn^{2+} , Ca^{2+} , CO_2^- , HCO_3^- , Mg^{2+} , Mn^{2+} , Mo^{2+} , K^+ , O_2 , NO_3^{2-} , P_i and SO_4 were allowed to freely enter and leave the network. Unconstrained uptake/secretion is represented in *i*JN678 by lower/upper bounds of $\pm 10^3$ mmol/gDW/h. In each individual simulation, all other external metabolites were only allowed to leave the system by constraining their exchange fluxes between $[0, 10^3]$ mmol/gDW/h, unless otherwise noted.

6. Simulation constraints

Growth rate performance. The following simulations were carried out in the *i*BG-11 minimal medium. Autotrophic metabolism was simulated by constraining the CO_2 or HCO_3^- exchange fluxes between $[-3.7, 10^3]$ mmol/gDW/h in accordance with the maximum CO_2 uptake rate estimated by (18). The photon uptake rate was constrained between $[-100, 0]$ mmol/gDW/h which corresponds to maximum irradiation of 24 to 39 $\mu\text{E m}^{-2} \cdot \text{s}^{-1}$ for photosynthesis yields of 6% or 4.6% respectively (40). Heterotrophic metabolism using glucose as the sole carbon source was simulated by constraining its exchange flux between $[-0.85, 10^3]$ mmol/gDW/h in accordance with the glucose uptake rate reported by (37) and photon uptake to 0 mmol/gDW/h. Mixotrophic metabolism was simulated by constraining the uptake rates of CO_2 (HCO_3^-), glucose and photons to 3.7, 0.38 and 100 mmol/gDW/h respectively. In the experiments involving internal flux distribution and growth rate predictions, mixotrophic conditions were simulated by constraining the *C_i* uptake rate to 0 according the culture conditions described by Yang et al (37).

Study of proton flux exchange in Synechocystis. The relative growth rates under autotrophic conditions using CO₂ and HCO₃, as well as under the mixo- and heterotrophic conditions described above, were computed as a function of proton flux exchange by constraining the H⁺ exchange fluxes between [-6, 4] mmol/gDW/h.

Expansion of the known array of carbon- and nitrogen sources which support growth. For the evaluation of potential carbon sources, the glucose uptake rate from the heterotrophic and mixotrophic conditions was constrained to 0 and the exchange fluxes for each potential carbon source i were changed between $v_{i,\min} \geq -1$ and $v_{i,\max} \geq 1000$ mmol/gDW/h. For the evaluation of potential nitrogen sources, the NO₃ uptake rate was set to zero and glucose used as the sole carbon source in heterotrophic and mixotrophic simulations. The potential nitrogen sources were allowed to enter the network freely (lower bounds of -10^3). A growth rate of at least 10% of the growth obtained with glucose and NO₃ was taken as an indication of growth.

For the evaluation of potential new carbon sources, the glucose uptake rate from the heterotrophic and mixotrophic simulations was constrained to zero and a cytoplasmatic sink reaction for each metabolite included in the reconstruction was added to the network. A lower bound of -1 mmol/gDW/h for each sink reaction was used, and the relative growth rate by carbon atom compared with hetero- or mixotrophic growth at the expense of glucose (lower bound of -1) was computed.

7. Gene essentiality and synthetic lethal analysis

The minimum number of genes required to sustain growth was studied under autotrophic, mixotrophic and heterotrophic conditions using the simulation procedure from (49, 50). A single simulation starts with a full network and selects a gene at random. If removal of this particular gene results in a viable network, the gene is permanently removed. The process is repeated for all the genes in the network. The remaining genes are essential for network survival. On the basis of 1000 simulation runs, sets of always-present genes (essential), sometimes-present genes (synthetic lethal) and never-present (nonessential) were identified. The network viability criterion was a minimum growth rate of 10% of the wild-type growth. For autotrophic growth, the carbon dioxide uptake was set to 3.7 mmol/gDW/h and the photon uptake to 100

mmol/gDW/h. For mixotrophic growth, glucose was added to the system by allowing an uptake corresponding to 0.85 mmol/gDW/h. For heterotrophic growth, light uptake was set to zero and glucose uptake to 0.85 mmol/gDW/h.

8. A simplified model used for photosynthesis analysis

The photosynthetic apparatus modeling of *Synechocystis* in *iJN678* accounts for equivalent reactions placed in different compartments as well as the broad use of alternative cofactors based on experimental evidence (Fig. S1, Dataset S1). In order to simplify the photosynthesis analysis, only photosynthetic reactions placed in the thylakoid membrane were allowed, and only one electron carrier was allowed. For this, the following constraints were applied:

- Since the blue copper protein plastocyanin (PC) and the heme protein cytochrome c6 (CytC) perform the same function in the photosynthetic electron-transport chain (39, 83), only PC was allowed as a soluble electron carrier, accepting electrons from cytochrome b₆f to reduce PSI. Thus, the fluxes across reactions CBFC2, PSI_2 and CYO1b_syn were constrained to zero (Fig. S1, Dataset S1).
- The NDH-1 complex can accept electrons from both NADPH and NADH (84). Since a specific NADH dehydrogenase was included in the reconstruction (NDH-2), only NADPH was allowed as an electron donor to the NDH-1 complex in order to simplify the analysis. For this, the fluxes across reactions NDH1_2u and NDH1_2p were constrained to zero (Fig. S1, Dataset S1).
- Only the reactions placed in the thylakoid membrane were allowed. The fluxes across reactions NDH1_1p, CYO1b2pp_syn, CYO1bpp_syn, CBFCpp and CYTBDpp were therefore constrained to zero (Fig. S1, Dataset S1).
- The reaction ferredoxin NADP⁺ reductase (FNOR) (EC: 1.18.1.2) was assumed to be irreversible under autotrophic conditions.

The following COBRA commands (14, 85) were used in order to apply the constraints to the model.

```
initCobraToolbox
model = xls2model ('Dataset S1.xlsx');
```

%Autotrophic conditions

```
model = changeObjective (model, 'Ec_biomass_SynAuto');
model = changeRxnBounds (model, 'EX_photon(e)', -100,'l');
model = changeRxnBounds (model, 'EX_glc(e)', 0,'l');
model = changeRxnBounds (model, 'EX_hco3(e)',-3.7,'l');
%Computing growth rate
sol=optimizeCbModel(model)
%sol = f: 0.0884
```

%Simplified photosynthetic model

```
%Constraining cytochrome c6-dependent reactions.
model = changeRxnBounds(model, 'CBFC2',0, 'b');
model = changeRxnBounds(model, 'PSI_2',0, 'b');
model = changeRxnBounds(model, 'CYO1b_syn',0, 'b');
```

```
%Constraining NADH-dependent reactions.
model = changeRxnBounds(model, 'NDH1_2u',0, 'b');
model = changeRxnBounds(model, 'NDH1_2p',0, 'b');
```

```
%Constraining peryplasmatic reactions.
model = changeRxnBounds(model, 'NDH1_1p',0, 'b');
model = changeRxnBounds(model, 'CYO1b2pp_syn',0, 'b');
model = changeRxnBounds(model, 'CYO1bpp_syn',0, 'b');
model = changeRxnBounds(model, 'CBFCpp',0, 'b');
model = changeRxnBounds(model, 'CYTBDpp',0, 'b');
```

```
%Assumed irreversibility of ferredoxin NADPH reductase under autotrophic conditions.
```

```
model = changeRxnBounds(model, 'FNOR',0, 'l');
%Assumed no excretion of CO2 under autotrophic conditions
model = changeRxnBounds (model, 'EX_co2(e)',0,'u');
```

%Model constraints applied to generate Figure 1

By using the simplified photosynthetic model, we constrained to zero the lower and upper bounds of the all AEF pathways identified.

%Building a model lacking AEF pathways

```
%Constraining NDH-1
model = changeRxnBounds(model, 'NDH1_1u',0, 'b');
```

```

%Constraining NDH-2
model = changeRxnBounds(model, 'NDH2_syn',0, 'b');
%Constraining NDH-13. NDH-14 is homologous reaction to NDH-13 but placed in
periplasm.
model = changeRxnBounds(model, 'NDH1_3u',0, 'b');
%Constraining FQR
model = changeRxnBounds(model, 'FQR',0, 'b');
%Constraining CYO
model = changeRxnBounds(model, 'CYO1b2_syn',0, 'b');
%Constraining CydBD
model = changeRxnBounds(model, 'CYTBDu',0, 'b');
%Constraining H2ase
model = changeRxnBounds(model, 'H2ASE_syn',0, 'b');
%Constraining MEHLER
model = changeRxnBounds(model, 'MEHLER',0, 'b');

```

Photorespiratory metabolism was constrained by constraining the oxygenic and carboxygenic activity of RuBisCO to minimum flux, which sustains maximum growth rate (0.0884).

% Building a model with the photorespiratory metabolism constrained

```

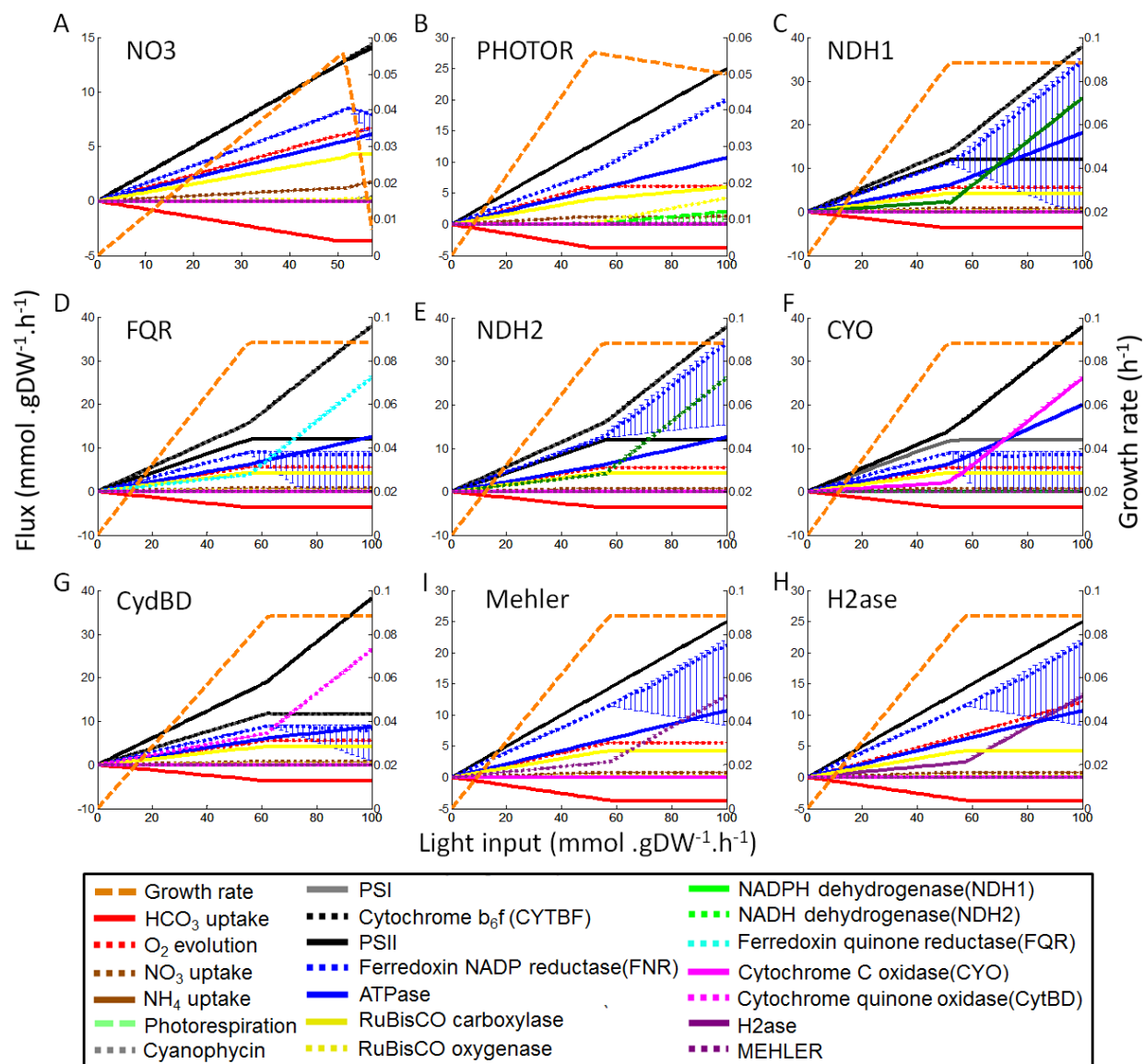
%Costraining Carboxygenic activity of RuBisCO
model = changeRxnBounds(model, 'RBPC',4.30987, 'u')
%Constraining Oxygenic activity of RuBisCO
model = changeRxnBounds(model, 'RBCh',0.2045310, 'u');

```

Computation of the functional states exhibited by *iJN678* when employing one AEF at a time was done by restoring the original bounds of each AEF pathway studied (Fig. 1C-I).

9. Robustness analysis of photosynthesis.

When FBA is applied to metabolic networks there are in general infinitely many flux distributions corresponding to the maximum cellular objective. Which flux distribution is obtained, depends on the particular LP solver used. To investigate how the presence of such alternate solutions affects our results, we computed the minimum and maximum possible flux through each of the reactions presented in Fig. 1 with fixed light uptake and growth rate (Fig. S11). With the exception of the FNR reaction and photorespiration in the CLS, there was essentially no variation which suggests that our results are robust to different attainable solutions. The large variation in FNR (which produces one mole of NADPH from 2 moles of reduced ferredoxin) is explained by the fact that multiple reactions included in the model can be used for converting between reducing equivalents. For instance, in the NH_4 fixation pathway, the reactions GLUS_x, GLUD_y, GLMS_{syn} and GLNS can work cooperatively, producing NAD(P)H from ferredoxin thus partially overcoming the role of FNR. However, these reactions don't result in net reducing equivalents consumption and they are well regulated *in vivo*. If it is assumed that GLUD_y only works in the reverse direction (it is mainly involved in nh_4 fixation rather than glutamate dehydrogenation) the variation in FNR decreases significantly. The small variation in PHOTOR is due to the presence of redundant photo-respiration pathways. In summary, we conclude that our results are robust towards the presence of alternate optima.



10. Estimation of ATP/NADPH ratio

Under non-photorespiratory conditions

The quantification of the photosynthetic parameters exhibited by AEF pathways is extensively detailed in Dataset S6. Briefly, all the reducing power from PSI was taken as NADPH (Flux_{PSI}) and 3 x flux across the ATPSu reaction was considered as the total ATP production ($3 \times \text{Flux}_{\text{ATPSu}}$) (86).

- NADPH consumption by NDH-1, NDH-1₃, NDH-2, FQR, MEHLER and H2ase

The total NADPH consumed by these pathways was calculated, taking into account that 1 mmol/gDW/h of NADPH is consumed per flux unit across these pathways (Flux_i), where i = NDH-1, NDH-1₃, NDH-2, FQR, MEHLER or H2ase.

- Net NADPH levels yield by AEF pathways

The remaining NADPH levels were calculated by subtracting the NADPH consumed from the total NADPH levels produced by PSI.

$\text{Net}_{\text{NADPHnp}} = \text{Flux}_{\text{PSI}} - \text{Flux}_i$ where $\text{Net}_{\text{NADPHnp}}$ = net NADPH produced (mmol/gDW/h) under non-photorespiratory conditions.

For CYO and CydBD, the NADPH from PSI was assumed as total NADPH produced, since these reactions accept electrons before passing them to PSI, e.g., from plastocyanin/cytochrome c6 and plastoquinone respectively (Fig. S1).

- Net ATP levels yield by AEF pathways

$\text{Net}_{\text{ATPnp}} = 3 \times \text{Flux}_{\text{ATPSu}}$, where $\text{Net}_{\text{ATPnp}}$ = net ATP produced (mmol/gDW/h) under non-photorespiratory conditions.

- ATP/NADPH ratio under non-photorespiratory conditions

$$\text{Net}_{\text{ATPnp}} / \text{Net}_{\text{NADPHnp}}$$

Under photorespiratory conditions

Under photorespiratory conditions, 2 ATP and one NADPH are necessary to produce 1 Glyceraldehyde-3P + 1 CO₂ from two 2-phosphoglycolate (87).

$\text{Flux}_{\text{PHOTOR}}$ = Fluxes across photorespiratory pathways (TRSARr or GLYCL, Dataset S1).

Additionally, 3 ATP and 2 NADPH are required for the re-fixing of the CO_2 produced.

- NADPH consumption by photorespiratory pathways

$\text{cNADPH}_{\text{ph}} = \text{Flux}_{\text{PHOTOR}}$, where $\text{cNADPH}_{\text{ph}}$ = NADPH consumed (mmol/gDW/h) under photorespiratory conditions.

- Net NADPH levels yield by photorespiratory pathways

$\text{Net}_{\text{NADPHph}} = \text{Flux}_{\text{PSI}} - \text{cNADPH}_{\text{ph}}$, where $\text{Net}_{\text{NADPHph}}$ = net NADPH produced (mmol/gDW/h) under photorespiratory conditions.

- ATP consumption by photorespiratory pathways

$\text{cATP}_{\text{ph}} = 2 \text{ Flux}_{\text{PHOTOR}}$, where cATP_{ph} is the ATP consumed (mmol/gDW/h) under photorespiratory conditions.

- Net ATP levels yield by photorespiratory pathways

$\text{Net}_{\text{ATPph}} = 3\text{Flux}_{\text{ATPSu}} - \text{cATP}_{\text{ph}}$, where $\text{Net}_{\text{ATPph}}$ = net ATP produced (mmol/gDW/h) under photorespiratory conditions.

- ATP/NADPH ratio under photorespiratory conditions

$\text{Net}_{\text{ATPph}} / \text{Net}_{\text{NADPHph}}$

Under extra NO_3 reduction conditions

Five NADPH (ten reduced ferredoxin) and 1 ATP are required to reduce NO_3 to NH_4 and the further fixation of this last compound into glutamine (88). In the absence of AEF pathways and extra reduction, fixation of NO_3 was computed (Fig. 2).

$\Delta\text{Flux}_{\text{NOR}} = \text{NOR} - \text{NOR}_{\text{AEF}}$, where $\Delta\text{Flux}_{\text{NOR}}$ is the increments in the flux across the nitrite reductase (NOR_{syn} , Dataset S1) under extra NO_3 reduction conditions, NOR the flux across NOR_{syn} in the absence of AEF pathways and NOR_{AEF} the flux across NOR_{syn} in the presence of AEF pathways.

- NADPH consumption by extra NO_3 reduction

$\text{cNADPH}_{\text{NO}_3} = 5 \text{ Flux}_{\text{NOR}}$, where $\text{cNADPH}_{\text{NO}_3}$ = NADPH consumed (mmol/gDW/h) under extra NO_3 reduction conditions.

- Net NADPH levels yield extra NO_3 reduction

$\text{Net}_{\text{NADPHNO}_3} = \text{Flux}_{\text{PSI}} - \text{cNADPH}_{\text{NO}_3}$, where $\text{Net}_{\text{NADPHNO}_3}$ = net NADPH produced (mmol/gDW/h) under extra NO_3 reduction conditions.

- ATP consumption by extra NO_3 reduction

$\text{cATP}_{\text{NO}_3} = \Delta \text{Flux}_{\text{NOR}}$, where $\text{cATP}_{\text{NO}_3}$ is the ATP consumed (mmol/gDW/h) under extra NO_3 reduction conditions.

- ATP consumption by cyanophycins biosynthesis (2x DM_cyanophy)

$\text{cATP}_{\text{cya}} = 2 \times \text{Flux}_{\text{cyan}}$, where cATP_{cya} is the ATP consumed (mmol/gDW/h) by cyanophycins biosynthesis.

- Net ATP levels yield by extra NO_3 reduction

$\text{Net}_{\text{ATPNO}_3} = 3\text{Flux}_{\text{ATPSu}} - (\text{cATP}_{\text{NO}_3} + \text{cATP}_{\text{cya}})$, where $\text{Net}_{\text{ATPNO}_3}$ = net ATP produced (mmol/gDW/h) under extra NO_3 reduction conditions.

- ATP/NADPH ratio under extra NO_3 reduction conditions

$\text{Net}_{\text{ATPNO}_3} / \text{Net}_{\text{NADPHNO}_3}$

11. Sequence data analysis

A homology search with completed cyanobacterial genomes was performed with the BLASTP algorithm (89) at the Cyanobase server (<http://genome.kazusa.or.jp/cyanobase>). The template proteins used in the analysis of the GABA shunt, TCA cycle and glucose transporter in cyanobacteria were:

- Glutamate decarboxylase (GLUCD) (EC: 4.1.1.15): GadB (b1419) from *E. coli*.
- 4-aminobutyrate aminotransferase (ABTA) (EC: 2.6.1.19): ABAT from *Homo sapiens* (18), PuuE (b1302) and GabT (b2662) from *E. coli*.
- Succinate-semialdehyde dehydrogenase (SSALyr) (EC: 1.2.1.16): GabD (b2661) from *E. coli*.
- 2-oxoglutarate decarboxylase complex (AKGDH): SucA (b0726) and SucB (b0727) from *E. coli*.
- Isocitrate lyase (ICL) (EC:4.1.3.1): AceA (b4015) from *E. coli*.
- Malate synthase (MS) (EC: 2.3.3.9): AceB (b4014) from *E. coli*.
- Glucose transport (GLCt2pp): GlcP (sll0771) from *Synechocystis*.

Supplementary References

1. Cooley JW & Vermaas WFJ (2001) Succinate Dehydrogenase and Other Respiratory Pathways in Thylakoid Membranes of *Synechocystis* sp. Strain PCC 6803: Capacity Comparisons and Physiological Function. *J. Bacteriol.* 183(14):4251-4258.
2. Ogawa T & Mi H (2007) Cyanobacterial NADPH dehydrogenase complexes. *Photosynthesis Research* 93(1):69-77.
3. Howitt CA & Vermaas WF (1998) Quinol and cytochrome oxidases in the cyanobacterium *Synechocystis* sp. PCC 6803. *Biochemistry* 37(51):17944-17951.
4. Allen JF (2002) Photosynthesis of ATP--Electrons, Proton Pumps, Rotors, and Poise. *Cell* 110(3):273-276.
5. Howitt C, Cooley J, Wiskich J, & Vermaas W (2001) A strain of *Synechocystis* sp. PCC 6803 without photosynthetic oxygen evolution and respiratory oxygen consumption: implications for the study of cyclic photosynthetic electron transport. *Planta* 214(1):46-56.
6. Yermenko N, *et al.* (2005) Open Reading Frame *ssr2016* is Required for Antimycin A-sensitive Photosystem I-driven Cyclic Electron Flow in the Cyanobacterium *Synechocystis* sp. PCC 6803. *Plant and Cell Physiology* 46(8):1433-1436.
7. Helman Y, *et al.* (2003) Genes Encoding A-Type Flavoproteins Are Essential for Photoreduction of O₂ in Cyanobacteria. *Current Biology* 13(3):230-235.
8. Germer F, *et al.* (2009) Overexpression, Isolation, and Spectroscopic Characterization of the Bidirectional [NiFe] Hydrogenase from *Synechocystis* sp. PCC 6803. *Journal of Biological Chemistry* 284(52):36462-36472.
9. Price GD, Badger MR, Woodger FJ, & Long BM (2008) Advances in understanding the cyanobacterial CO₂-concentrating-mechanism (CCM): functional components, Ci transporters, diversity, genetic regulation and prospects for engineering into plants. *Journal of Experimental Botany* 59(7):1441-1461.
10. Eisenhut M, *et al.* (2008) The photorespiratory glycolate metabolism is essential for cyanobacteria and might have been conveyed endosymbiontically to plants. *Proceedings of the National Academy of Sciences* 105(44):17199-17204.
11. Schäfer L, Vioque A, & Sandmann G (2005) Functional in situ evaluation of photosynthesis-protecting carotenoids in mutants of the cyanobacterium *Synechocystis* PCC6803. *Journal of Photochemistry and Photobiology B: Biology* 78(3):195-201.
12. DellaPenna D & Pogson BJ (2006) VITAMIN SYNTHESIS IN PLANTS: Tocopherols and Carotenoids. *Annual Review of Plant Biology* 57(1):711-738.
13. Wang F, Jiang JG, & Chen Q (2010) Progress on molecular breeding and metabolic engineering of biosynthesis pathways of C30, C35, C40, C45, C50 carotenoids. *Biotechnology Advances* 25(3):211-222.
14. Thiele I & Palsson BO (2010) A protocol for generating a high-quality genome-scale metabolic reconstruction. *Nat. Protocols* 5(1):93-121.
15. Liu X, Sheng J, & Curtiss III R (2011) Fatty acid production in genetically modified cyanobacteria. *Proceedings of the National Academy of Sciences* 108(17):6899-6904.
16. Okazaki K, Sato N, Tsuji N, Tsuzuki M, & Nishida I (2006) The Significance of C16 Fatty Acids in the sn-2 Positions of Glycerolipids in the Photosynthetic Growth of *Synechocystis* sp. PCC6803. *Plant Physiol.* 141(2):546-556.

17. Tasaka Y, *et al.* (1996) Targeted mutagenesis of acyl-lipid desaturases in *Synechocystis*: evidence for the important roles of polyunsaturated membrane lipids in growth, respiration and photosynthesis. *EMBO Journal* 15(23):6416-6425.
18. Shastri AA & Morgan JA (2005) Flux Balance Analysis of Photoautotrophic Metabolism. *Biotechnology Progress* 21(6):1617-1626.
19. Fu P (2009) Genome-scale modeling of *Synechocystis* sp. PCC6803 and prediction of pathway insertion. *Journal of Chemical Technology & Biotechnology* 84:473 - 483.
20. Knoop H, Zilliges Y, Lockau W, & Steuer R (2010) The Metabolic Network of *Synechocystis* sp. PCC 6803: Systemic Properties of Autotrophic Growth. *Plant Physiology* 154(1):410-422.
21. Montagud A, *et al.* (2011) Flux coupling and transcriptional regulation within the metabolic network of the photosynthetic bacterium *Synechocystis* sp. PCC6803. *Biotechnology Journal* 6(3):330-342.
22. Montagud A, Navarro E, Fernandez de Cordoba P, Urchueguia J, & Patil K (2010) Reconstruction and analysis of genome-scale metabolic model of a photosynthetic bacterium. *BMC Syst Biol* 4(1):156.
23. Luque I & Forchhammer K (2008) Nitrogen Assimilation and C/N Balance Sensing. *The Cyanobacteria. Molecular Biology, Genomics and Evolution*, eds Herrero A & Flores E (Caister Academic Press, Norfolk, UK), pp 335-382.
24. Laudenbach DE & Grossman AR (1991) Characterization and mutagenesis of sulfur-regulated genes in a cyanobacterium: evidence for function in sulfate transport. *J. Bacteriol.* 173(9):2739-2750.
25. Pitt FD, Mazard S, Humphreys L, & Scanlan DJ (2010) Functional Characterization of *Synechocystis* sp. Strain PCC 6803 *pst1* and *pst2* Gene Clusters Reveals a Novel Strategy for Phosphate Uptake in a Freshwater Cyanobacterium. *J. Bacteriol.* 192(13):3512-3523.
26. Quintero MJ, Montesinos ML, Herrero A, & Flores E (2001) Identification of Genes Encoding Amino Acid Permeases by Inactivation of Selected ORFs from the *Synechocystis* Genomic Sequence. *Genome Research* 11(12):2034-2040.
27. Schmetterer G (1990) Sequence conservation among the glucose transporter from the cyanobacterium *Synechocystis* sp. PCC 6803 and mammalian glucose transporters. *Plant Mol Biol* 14(5):697-706.
28. Koksharova O, Schubert M, Shestakov S, & Cerff R (1998) Genetic and biochemical evidence for distinct key functions of two highly divergent GAPDH genes in catabolic and anabolic carbon flow of the cyanobacterium *Synechocystis* sp. PCC 6803. *Plant Molecular Biology* 36(1):183-194.
29. Bricker TM, *et al.* (2004) The Malic Enzyme Is Required for Optimal Photoautotrophic Growth of *Synechocystis* sp. Strain PCC 6803 under Continuous Light but Not under a Diurnal Light Regimen. *J. Bacteriol.* 186(23):8144-8148.
30. Cooley JW, Howitt CA, & Vermaas WFJ (2000) Succinate:Quinol Oxidoreductases in the Cyanobacterium *Synechocystis* sp. Strain PCC 6803: Presence and Function in Metabolism and Electron Transport. *J. Bacteriol.* 182(3):714-722.
31. Tamber S & Hancock REW (2004) The outer membranes of pseudomonads. *Pseudomonas*, ed Ramos JL (Kluwer Academic, New York), Vol 1, pp 575-601.
32. Reed JL, Vo TD, Schilling CH, & Palsson BO (2003) An expanded genome-scale model of *Escherichia coli* K-12 (iJR904 GSM/GPR). *Genome Biology* 4(9):R54.51 - R54.52.

33. Feist AM & Palsson BO (2010) The biomass objective function. *Current Opinion in Microbiology* 13(3):344-349.
34. Janssen P, Goldovsky L, Kunin V, Darzentas N, & Ouzounis C (2005) Genome coverage, literally speaking. The challenge of annotating 200 genomes with 4 million publications. *EMBO Rep* 6(5):397-399.
35. Hong SJ & Lee CG (2007) Evaluation of central metabolism based on a genomic database of *Synechocystis* sp. PCC6803. *Biotechnology and Bioprocess Engineering* 12(2):165-173.
36. Navarro E, Montagud A, Fernández de Córdoba P, & Urchueguía JF (2009) Metabolic flux analysis of the hydrogen production potential in *Synechocystis* sp. PCC6803. *International Journal of Hydrogen Energy* 34(21):8828-8838.
37. Yang C, Hua Q, & Shimizu K (2002) Metabolic flux analysis in *Synechocystis* using isotope distribution from ¹³C-labeled glucose. *Metab Eng* 4:202 - 216.
38. Emlyn-Jones D, Ashby M, & Mullineaux C (1999) A gene required for the regulation of photosynthetic light harvesting in the cyanobacterium *Synechocystis* 6803. *Mol Microbiol* 33:1050-1058.
39. Eriksen N, Riisgård F, Gunther W, & Iversen JJJ (2007) On-line estimation of O₂; production, CO₂; uptake, and growth kinetics of microalgal cultures in a gas-tight photobioreactor. *Journal of Applied Phycology* 19(2):161-174.
40. Zhu X-G, Long SP, & Ort DR (2008) What is the maximum efficiency with which photosynthesis can convert solar energy into biomass? *Current Opinion in Biotechnology* 19(2):153-159.
41. Foster J, Singh A, Rothschild L, & Sherman L (2007) Growth-phase dependent differential gene expression in *Synechocystis* sp. strain PCC 6803 and regulation by a group 2 sigma factor. *Archives of Microbiology* 187(4):265-279.
42. Shastri AA & Morgan JA (2007) A transient isotopic labeling methodology for ¹³C metabolic flux analysis of photoautotrophic microorganisms. *Phytochemistry* 68(16-18):2302-2312.
43. Pelroy RA, Rippka R, & Stanier RY (1972) Metabolism of glucose by unicellular blue-green algae. *Arch Mikrobiol* 87(4):303-322.
44. Stal LJ & Moezelaar R (1997) Fermentation in cyanobacteria. *FEMS Microbiology Reviews* 21(2):179-211.
45. Young JD, Shastri AA, Stephanopoulos G, & Morgan JA (2011) Mapping photoautotrophic metabolism with isotopically nonstationary ¹³C flux analysis. *Metabolic Engineering* 13(6):656-665.
46. Owittrim G & Colman B (1988) Phosphoenolpyruvate carboxylase mediated carbon flow in a cyanobacterium. *Biochem. Cell Biol* 66:93-99.
47. Kim HW, Vannela R, Zhou C, & Rittmann BE (2011) Nutrient acquisition and limitation for the photoautotrophic growth of *Synechocystis* sp. PCC6803 as a renewable biomass source. *Biotechnology and Bioengineering* 108(2):277-285.
48. Srinivasan K & Mahadevan R (2010) Characterization of proton production and consumption associated with microbial metabolism. *BMC Biotechnology* 10(1):2.
49. Zhang Y, *et al.* (2009) Three-Dimensional Structural View of the Central Metabolic Network of *Thermotoga maritima*. *Science* 325(5947):1544-1549.
50. Pál C, *et al.* (2006) Chance and necessity in the evolution of minimal metabolic networks. *Nature* 440(7084):667-670.

51. Nakao M, *et al.* (2010) CyanoBase: the cyanobacteria genome database update 2010. *Nucleic Acids Research* 38(suppl 1):D379-D381.
52. Fernández-González B, Sandmann G, & Vioque A (1997) A New Type of Asymmetrically Acting β -Carotene Ketolase Is Required for the Synthesis of Echinenone in the Cyanobacterium *Synechocystis* sp. PCC 6803. *Journal of Biological Chemistry* 272(15):9728-9733.
53. Lagarde D, Beuf L, & Vermaas W (2000) Increased production of zeaxanthin and other pigments by application of genetic engineering techniques to *Synechocystis* sp. strain PCC 6803. *Appl Environ Microbiol* 66:64-72.
54. Lee JM, *et al.* (2005) Identification of a glucokinase that generates a major glucose phosphorylation activity in the cyanobacterium *Synechocystis* sp. PCC 6803. *Mol Cells* 19(2):256-261.
55. Astier C, Elmorjani K, Meyer I, Joset F, & Herdman M (1984) Photosynthetic mutants of the cyanobacteria *Synechocystis* sp. strains PCC 6714 and PCC 6803: sodium p-hydroxymercuribenzoate as a selective agent. *J Bacteriol* 158:659-664.
56. Osiewacz H (1992) Construction of insertion mutants of *Synechocystis* sp. PCC 6803: Evidence for an essential function of subunit IV of the cytochrome b6/f complex. *Arch Microbiol* 157(4):336-342.
57. Kitano H (2004) Biological robustness. *Nat Rev Genet* 5(11):826-837.
58. Oliveros JC (2007) VENNY. An interactive tool for comparing lists with Venn Diagrams. in <http://bioinfogp.cnb.csic.es/tools/venny/>.
59. Chen G-Q & Chen F (2006) Growing Phototrophic Cells without Light. *Biotechnology Letters* 28(9):607-616.
60. Anderson SL & McIntosh L (1991) Light-activated heterotrophic growth of the cyanobacterium *Synechocystis* sp. strain PCC 6803: a blue-light-requiring process. *J. Bacteriol.* 173(9):2761-2767.
61. Panda B & Mallick N (2007) Enhanced poly- β -hydroxybutyrate accumulation in a unicellular cyanobacterium, *Synechocystis* sp. PCC 6803. *Letters in Applied Microbiology* 44(2):194-198.
62. Raksajit W, Mäenpää P, & Incharoensakdi A (2006) Putrescine transport in a cyanobacterium *Synechocystis* sp. PCC 6803. *J Biochem Mol Biol* 39(4):394-399.
63. Raksajit W, Yodsang P, Maenpaa P, & Incharoensakdi A (2009) Characterization of spermidine transport system in a cyanobacterium, *synechocystis* sp. PCC 6803. *J Microbiol Biotechnol* 19(5):447-454.
64. Hagemann M, Richter S, & Mikkat S (1997) The *ggtA* gene encodes a subunit of the transport system for the osmoprotective compound glucosylglycerol in *Synechocystis* sp. strain PCC 6803. *J. Bacteriol.* 179(3):714-720.
65. Mikkat S & Hagemann M (2000) Molecular analysis of the *ggtBCD* gene cluster *Synechocystis* sp. strain PCC6803 encoding subunits of an ABC transporter for osmoprotective compounds. *Archives of Microbiology* 174(4):273-282.
66. Kaneko T, *et al.* (1996) Sequence Analysis of the Genome of the Unicellular Cyanobacterium *Synechocystis* sp. Strain PCC6803. II. Sequence Determination of the Entire Genome and Assignment of Potential Protein-coding Regions. *DNA Research* 3(3):109-136.
67. Kanehisa M, *et al.* (2006) From genomics to chemical genomics: new developments in KEGG. *Nucl Acids Res* 34(suppl_1):D354 - 357.

68. Caspi R, *et al.* (2010) The MetaCyc database of metabolic pathways and enzymes and the BioCyc collection of pathway/genome databases. *Nucl. Acids Res.* 38(suppl_1):D473-479.
69. Schomburg I, Chang A, & Schomburg D (2002) BRENDA, enzyme data and metabolic information. *Nucl. Acids Res.* 30(1):47-49.
70. Herrero A & Flores E (2008) *The cyanobacteria: Molecular Biology, Genomics and Evolution* (Caister Academic Press, Norfolk, UK).
71. Kato K, Tanaka R, Sano S, Tanaka A, & Hosaka H (2010) Identification of a gene essential for protoporphyrinogen IX oxidase activity in the cyanobacterium *Synechocystis* sp. PCC6803. *Proceedings of the National Academy of Sciences* 107(38):16649-16654.
72. Feist AM, *et al.* (2007) A genome-scale metabolic reconstruction for *Escherichia coli* K-12 MG1655 that accounts for 1260 ORFs and thermodynamic information. *Mol Syst Biol* 3.
73. Yoo S-H, Spalding MH, & Jane J-I (2002) Characterization of cyanobacterial glycogen isolated from the wild type and from a mutant lacking of branching enzyme. *Carbohydrate Research* 337(21-23):2195-2203.
74. Schledz M, Seidler A, Beyer P, & Neuhaus G (2001) A novel phytyltransferase from *Synechocystis* sp. PCC 6803 involved in tocopherol biosynthesis. *FEBS Lett* 499:15-20.
75. Nakamura A, Akai M, Yoshida E, Taki T, & Watanabe T (2003) Reversed-phase HPLC determination of chlorophyll *a'* and phylloquinone in Photosystem I of oxygenic photosynthetic organisms. *European Journal of Biochemistry* 270(11):2446-2458.
76. Neidhardt FC, Ingraham JL, & Schaechter M (1990) Physiology of the bacterial cell: a molecular approach.
77. Jantaro S, Mäenpää P, Mulo P, & Incharoensakdi A (2003) Content and biosynthesis of polyamines in salt and osmotically stressed cells of *Synechocystis* sp. PCC 6803. *FEMS Microbiol Lett* 228(1):129-135.
78. Price ND, Reed JL, & Palsson BO (2004) Genome-scale models of microbial cells: evaluating the consequences of constraints. *Nat Rev Microbiol* 2(11):886 - 897.
79. Varma A & Palsson BO (1994) Stoichiometric flux balance models quantitatively predict growth and metabolic by-product secretion in wild-type *Escherichia coli* W3110. *Appl Environ Microbiol* 60(10):3724-3731.
80. Mahadevan R & Schilling CH (2003) The effects of alternate optimal solutions in constraint-based genome-scale metabolic models. *Metabolic Engineering* 5(4):264-276.
81. Becker SA, *et al.* (2007) Quantitative Prediction of Cellular Metabolism with Constraint-based Models: The COBRA Toolbox. *Nat Protoc* 2(3):727 - 738.
82. Rippka R (1988) Isolation and purification of cyanobacteria. *Methods Enzymol* 167:3-27.
83. Ullmann GM, Hauswald M, Jensen A, & Knapp EW (2000) Structural alignment of ferredoxin and flavodoxin based on electrostatic potentials: Implications for their interactions with photosystem I and ferredoxin-NADP reductase. *Proteins* 38:301-309.
84. Matsuo M, Endo T, & Asada K (1998) Properties of the respiratory NAD(P)H dehydrogenase isolated from the cyanobacterium *Synechocystis* PCC6803. *Plant Cell Physiol* 39:263-267.
85. Becker S, *et al.* (2007) Quantitative Prediction of Cellular Metabolism with Constraint-based Models: The COBRA Toolbox. *Nat Protoc* 2(3):727 - 738.

86. Allen JF (2003) Cyclic, pseudocyclic and noncyclic photophosphorylation: new links in the chain. *Trends Plant Sci* 8(1):15-19.
87. Wingler A, Lea P, WP Q, & Leegood R (2000) Photorespiration: metabolic pathways and their role in stress protection. *Philos Trans R Soc Lond B Biol Sci* 355(1402):1517-1529.
88. Edwards G & Walker D (1983) *C3, C4: mechanisms, and cellular and environmental regulation, of photosynthesis* (Blackwell Scientific publications, Oxford).
89. Kaplan A, Hagemann M, Bauwe H, Kahlon S, & Ogawa T (2008) Carbon Acquisition by Cyanobacteria: Mechanisms, Comparative Genomics, and Evolution. *The Cyanobacteria. Molecular Biology, Genomics and Evolution*, eds Herrero A & Flores E (Caister Academic Press, Norfolk, UK), pp 305-334.